REPORT DOCUMENTATION PAGE				Form Approved OMB No. 0704-0188

1. AGENCY USE ONLY *(Leave blank)*	2. REPORT DATE December 1994	3. REPORT TYPE AND DATES COVERED Master's Thesis

4. TITLE AND SUBTITLE PRIME POWER FOR SHIPBOARD HIGH-AVERAGE POWER FELs	5. FUNDING NUMBERS
6. AUTHOR(S) Robert Allen Lyon Jr.	
7. PERFORMING ORGANIZATION NAME(S) AND ADDRESS(ES) Naval Postgraduate School Monterey CA 93943-5000	8. PERFORMING ORGANIZATION REPORT NUMBER
9. SPONSORING/MONITORING AGENCY NAME(S) AND ADDRESS(ES)	10. SPONSORING/MONITORING AGENCY REPORT NUMBER

11. SUPPLEMENTARY NOTES The views expressed in this thesis are those of the author and do not reflect the official policy or position of the Department of Defense or the U.S. Government.

12a. DISTRIBUTION/AVAILABILITY STATEMENT Approved for public release; distribution is unlimited.	12b. DISTRIBUTION CODE

13. ABSTRACT *(maximum 200 words)*

High-power free electron lasers (FELs), capable of deployment aboard naval combatants, would place a unique and significant demand upon the ship's electrical distribution system. A shipboard FEL must be power efficient, relatively compact, and present a minimum radiation hazard to nearby personnel. The feasibility of deploying an FEL aboard a ship is analyzed from a power system perspective.

To produce 1 MW of laser power, it is determined that 6.6 MW of high-voltage dc power is required to drive the FEL when superconductor accelerator technology is employed and 9 MW is required when conventional room temperature accelerator technology is used. The required prime power electrical distribution is easily compatible with the gas turbine engineering plants of modern surface combatants. This distribution will add 22 tons to the ship's displacement and require 22 m^3 of the ship's volume to implement. Simulation results show that the FEL would require an undulator with only 16 periods to produce 1 MW for the electron beam parameters developed during the power analysis. This FEL exhibits a large tolerance to electron beam quality. From a power analysis viewpoint, FELs may become a competitive technology for a prospective naval laser weapon.

14. SUBJECT TERMS Prime Power, Photocathode, Power Distribution			15. NUMBER OF PAGES 97
			16. PRICE CODE
17. SECURITY CLASSIFICATION OF REPORT Unclassified	18. SECURITY CLASSIFICATION OF THIS PAGE Unclassified	19. SECURITY CLASSIFICATION OF ABSTRACT Unclassified	20. LIMITATION OF ABSTRACT UL

NSN 7540-01-280-5500

Standard Form 298 (Rev. 2-89)
Prescribed by ANSI Std. 239-18 298-102

PRIME POWER FOR SHIPBOARD HIGH-AVERAGE POWER FELs

by

Robert A. Lyon Jr.
Lieutenant, United States Navy
B.S.E.E., United States Naval Academy, 1987

Submitted in partial fulfillment of the
requirements for the degrees of

MASTER OF SCIENCE IN APPLIED PHYSICS
MASTER OF SCIENCE IN ELECTRICAL ENGINEERING
from the
NAVAL POSTGRADUATE SCHOOL
December 1994

ABSTRACT

High-power free electron lasers (FELs), capable of deployment aboard naval combatants, would place a unique and significant demand upon the ship's electrical distribution system. A shipboard FEL must be power efficient, relatively compact, and present a minimum radiation hazard to nearby personnel. The feasibility of deploying an FEL aboard a ship is analyzed from a power system perspective.

To produce 1 MW of laser power, it is determined that 6.6 MW of high-voltage dc power is required to drive the FEL when superconductor accelerator technology is employed and 9 MW is required when conventional room temperature accelerator technology is used. The required prime power electrical distribution is easily compatible with the gas turbine engineering plants of modern surface combatants. This distribution will add 22 tons to the ship's displacement and require 22 m^3 of the ship's volume to implement. Simulation results show that the FEL would require an undulator with only 16 periods to produce 1 MW for the electron beam parameters developed during the power analysis. This FEL exhibits a large tolerance to electron beam quality. From a power analysis viewpoint, FELs may become a competitive technology for a prospective naval laser weapon.

Table of Contents

ACKNOWLEDGEMENT

The author is very grateful to George Neil and the Accelerator Department of the Continuous Electron Beam Accelerator Facility (CEBAF) and Professor Todd Smith of the Hansen Experimental Physics Laboratory at Stanford University for their efforts in assisting this project. Their contributions advanced this project considerably.

The author is especially grateful to Professor Bill Colson and Dr. Robert Wong for their assistance and guidance throughout this project. Their patience and insight was invaluable. Thanks are extended to Professors Bob Ashton and Bob Armstead for their advice, encouragement, and support.

Finally, this would not have been possible without the love and support of my wife, Suzi. Thank you.

I. INTRODUCTION

The free electron laser (FEL) was first proposed by J.M.J. Madey in 1971 [1] and lased in 1976 at Stanford University. The FEL technology was so promising that extensive funding and resources were devoted to FEL research as part of the Strategic Defense Initiative (SDI). Consequently, rapid developments in FEL theory and design were made throughout the 1980s. Currently, the technology has matured to where high-average power FELs are feasible. Stanford University, Boeing, Rocketdyne, and the Continuous Electron Beam Accelerator Facility (CEBAF) are among those pursuing kilowatt level FELs.

The simplified schematic of a generic FEL is depicted in Figure 1.

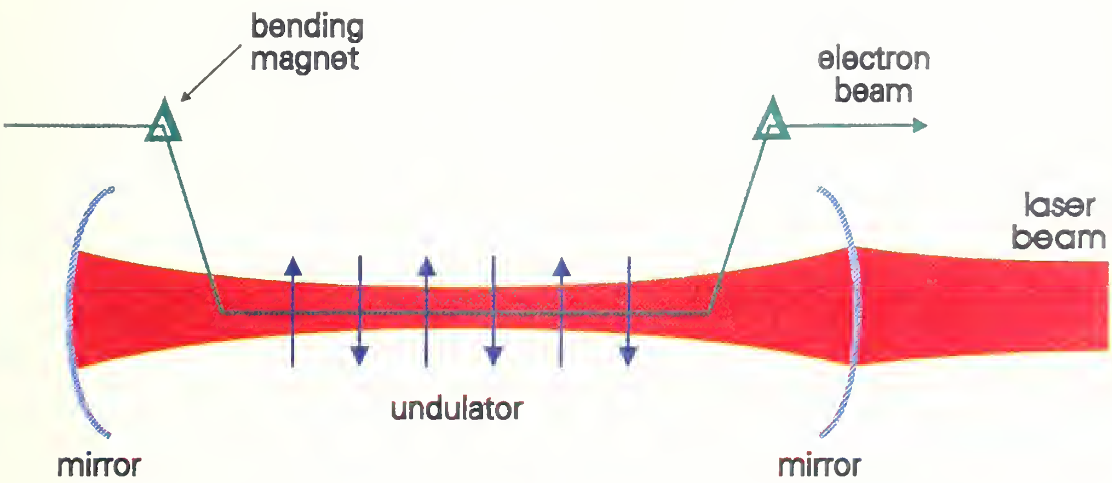

Figure 1 - Simplified FEL diagram

A relativistic electron beam is deflected periodically by an oscillating magnetic field produced by a series of magnets called the undulator. The electron beam consists of a series of picosecond electron pulses, called micropulses, separated in time with a duty cycle about 10^{-4}. Often the micropulses are produced in trains several microseconds long at repetition rates of a few hertz. One full cycle of this repetition is called a macropulse. However, continuous wave

(CW) operation of electron beams, where a continuous stream of micropulses are injected into the undulator, can also be used. Light is radiated from the accelerated electrons, collected in an optical resonator cavity, and then amplified by subsequent electron pulses.

Light recirculates within the optical resonator in pulses. The resonator cavity dimensions are aligned so that each optical pulse co-propagates with an electron micropulse as it travels down the length of the undulator. The micropulse is several hundred optical wavelengths long so that within a length of the micropulse corresponding to an optical wavelength, the electron longitudinal spatial distribution is essentially homogeneous.

FELs are an attractive light source for several reasons. Perhaps the most positive attribute of FELs is, unlike chemical or solid-state lasers, that the optical wavelength can be tuned over a wide range of wavelengths. The wavelength is a function of electron beam energy. With slight variations in the beam energy, the FEL wavelength can be tuned over a range of about an order of magnitude about the center wavelength. A more complete description of FEL theory is presented in Chapter II.

The FEL also has disadvantages. The average power of FELs has been limited to only a few watts while the capital cost of the FEL, including the undulator magnets and a radiofrequency (rf) accelerator system used to produce and transport the electron beam, can cost tens of millions of dollars. Electron accelerators have been unable to produce the large average currents required to generate high-average power. Technology will now support a kilowatt scale FEL and a 100 kW FEL is expected within 5-10 years [2].

Free electron lasers are of interest to the Department of Defense due to their potential as high-power weapons and lower power countermeasure devices. A shipboard high-power FEL could provide essentially a zero time-of-flight defense against enemy missiles and aircraft. The need for such a weapon has been previously established [3][4]. Technological developments required to build an FEL weapon, however, are probably more than ten years away.

A shipboard FEL would require an electrical prime power source. The amount and type of power required by an FEL would place a specific demand on a ship's electrical power distribution system. Several possible choices of FEL system architectures are potential candidates for a high-power FEL. The maritime combat environment, however, places unique design constraints on the system. In Chapter III, the power requirements of the FEL architecture most suited to this environment are described. The methods used to determine these requirements are also valid for other architectures with appropriate changes in design parameters. All of the technologies considered are in use on existing FELs or have otherwise been demonstrated. No attempt to predict future technologies has been made. Chapter IV

outlines the prime power considerations in producing and distributing this power for the shipboard engineering plants that will power naval combatants into the 21^{st} century.

The power analysis of Chapter III makes several assumptions that would affect the design and operation of the undulator and optical resonator. In Chapter V, simulations are presented to demonstrate that an FEL can operate at design levels under these assumptions. Current accelerator and optics technology, however, would not likely be able to support all of these parameters but it is important to validate the feasibility of pursuing such a design or a derivative.

This thesis incorporates many of the aspects of FEL design. An FEL is not comprised of a set of unique characteristics. There are many design choices which must be made in order to define a given FEL architecture. The feasibility of a high-power shipboard FEL weapon is examined from a power analysis approach. A model for an FEL weapon is defined based on the volume, power distribution, and environmental constraints of the maritime combat environment. The power requirements for this model are determined and the characteristics of the required power distribution system are outlined. Finally, the optical characteristics and performance of this FEL model is explored.

II. FREE ELECTRON LASER THEORY

The basic components of an FEL are a relativistic electron beam, a static periodic magnetic field, and a co-propagating optical field. The FEL operates through the quantum-mechanical processes of spontaneous emission, stimulated emission and stimulated absorption. The quantum-mechanical descriptions of these processes for bound electrons, as in an atomic laser, are well-known and easily formulated. It is not necessary, however, to use the quantum-mechanical descriptions for the FEL. The FEL can be completely described by classical electromagnetic theory relations since there is a high density of electrons within an FEL electron beam and photons within the optical wave [5]. The following theory has been collected from a variety of sources. The principal sources for each of the following sections are noted in the subject headings. The following relationships are presented in the cgs unit system.

A. RESONANCE CONDITION [5][6]

An accelerated electron radiates energy. In the FEL, the free electrons are accelerated by the static periodic magnetic field within the undulator. The electrons are traveling down the axis of the undulator at relativistic speeds. Therefore, the period (wavelength) of the magnetic fields as they appear to the electron are not the same as the apparent undulator period as seen by an observer in the laboratory frame. This is often referred to as the relativistic Doppler shift. Since the undulator wavelength as seen by the electrons is a function of their energy, the wavelength of the photons emitted by the electrons is also a function of their energy. We can describe these effects, however, within the laboratory frame of reference due to the relativistic invariance of our classical relationships [7].

The electron beam interactions with the electromagnetic fields within the laser cavity are described by the Lorentz equations and the wave equation. The relativistic form of the Lorentz equations are:

$$\frac{d}{dt}(\gamma mc\vec{\beta}) = -e(\vec{E} + \vec{\beta} \times \vec{B}) \tag{2.1}$$

$$\frac{d}{dt}(\gamma mc) = -e\,\vec{\beta} \cdot \vec{E} \tag{2.2}$$

$$\gamma = \frac{1}{\sqrt{1 - \vec{\beta} \cdot \vec{\beta}}} \tag{2.3}$$

where γ is the Lorentz factor, $\vec{\beta} = \vec{v}/c$, $\vec{v}$ is the electron velocity, c is the speed of light, m is the rest mass of an electron, e is elementary charge magnitude of an electron, $\vec{E}$ is the electric field within the laser cavity, and $\vec{B}$ is the total of magnetic fields within the laser cavity.

Equation 2.1 represents conservation of momentum for the system and is commonly known as the Lorentz force equation. Equation 2.2 describes energy transfer and would be called stimulated emission or absorption in a quantum-mechanical formulation. For an FEL we desire a net transfer of energy from the electron beam to the optical field that is initially produced from spontaneous emission. This energy transfer is many orders of magnitude larger than the spontaneous emission contribution per pass of the electron beam through the undulator. We must ensure that stimulated emission occurs preferentially to stimulated absorption in order to make the FEL a useful device.

The electric field, $\vec{E}$, within the undulator is due to the presence of the optical field. Equation 2.2 shows that for $\vec{v}\cdot\vec{E} > 0$, energy will be transferred from an electron to the optical field. Furthermore, special relativity states that the speed of an electron must be less than the speed of light in free space so that the electron must travel slower than ("slips" along) the co-propagating optical field. The transverse component of the electron velocity is periodic due to the acceleration of the electrons by the undulator. While traveling through one undulator wavelength, λ_o, the electron's transverse velocity, $v_\perp$, will oscillate one full period as shown in Figure 2. In this figure, an electron's longitudinal travel is shown with it's average velocity over one undulator wavelength, $\beta_{\|}c$. After one undulator period, the electron slips behind the optical wave by one optical wavelength, λ. At position z = 0, this electron is located where $\vec{E} = 0$ and $v_\perp = 0$. As the electron moves down the undulator, $v_\perp$ increases and $\vec{E}$ becomes positive so that $\vec{v}\cdot\vec{E} > 0$ from $0 < z < \lambda_o/2$. As the electron continues down the undulator, both $\vec{v}_\perp$ and $\vec{E}$ are less than zero so that $\vec{v}\cdot\vec{E} > 0$ from $\lambda_o/2 < z < \lambda_o$. The condition where the electron slips behind the optical wave by one optical wavelength as the electron traverses an undulator wavelength is called the resonance condition. A single resonant electron transfers energy from the beam to the optical field.

The resonance condition defines an important feature of the FEL; specifically, its wavelength tunability. To illustrate this, we begin with the Lorentz factor equation. Since $\vec{\beta}\cdot\vec{\beta} = \beta_z^2 + \beta_\perp^2$, the Lorentz factor (equation 2.3) can be rearranged to solve for

$$\beta_z = \sqrt{1 - (1 + \gamma^2\beta_\perp^2)\,/\,\gamma^2}\ . \tag{2.4}$$

Define $K^2 = \gamma^2\beta_\perp^2 \equiv$ undulator parameter. Typical values of K and γ are $K \approx 1$ and $\gamma \approx 50$-500 so that $1 + \gamma^2\beta_\perp^2/\gamma^2 << 1$. With a Taylor expansion, we have

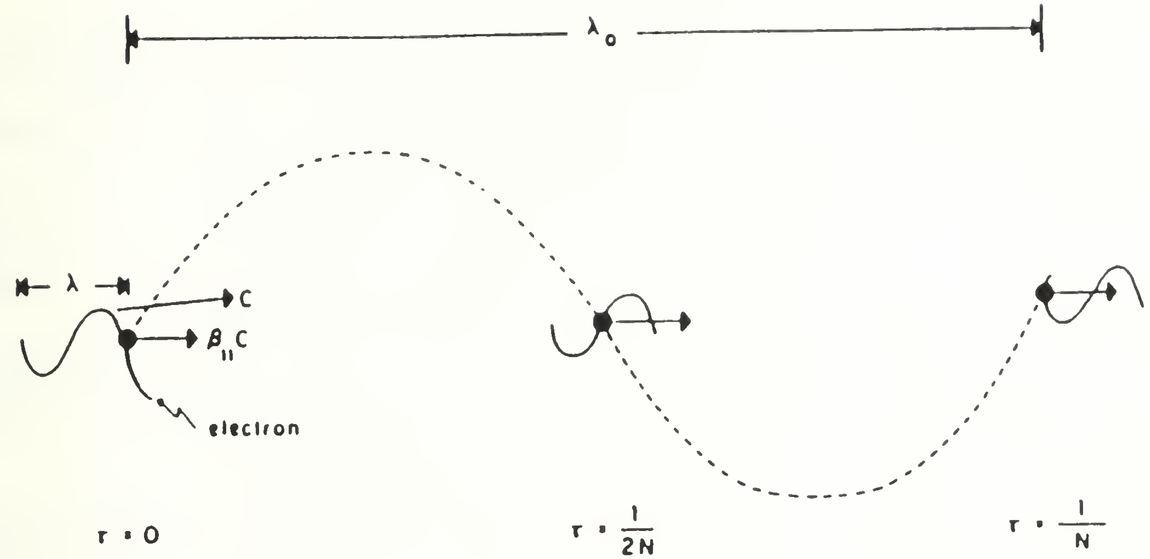

Figure 2 - Electron slippage of an optical wavelength as it traverses a distance of one undulator wavelength. From Ref. [4]

$$\beta_z \approx 1 - \frac{1 + K^2}{2\gamma^2} \; . \tag{2.5}$$

The difference in velocity between the optical wave and the electrons is $c(1-\beta_z)$, while the time it takes for the electron to traverse an undulator period is $\lambda_o/\beta_z c$. Therefore, the resonance condition is

$$\lambda = \lambda_o \; \frac{1 + K^2}{2\gamma^2} \; . \tag{2.6}$$

This mathematical representation of the resonance condition demonstrates the wavelength tunability of the FEL. In section II.C, we will see that

$$K = \frac{e\bar{B}_o \lambda_o}{2\pi mc^2} \tag{2.7}$$

where $\bar{B}_o$ is the undulator rms magnetic field strength. The undulator field strength and wavelength characteristics are fixed after undulator construction. Therefore, since $\lambda \propto 1/\gamma^2$, the FEL optical wavelength can be rapidly adjusted over a wide range with small adjustments to the electron energy. Actual FEL experiments have produced optical radiation at wavelengths of 10mm $\gtrsim \lambda \gtrsim$ 300nm [5].

B. SPONTANEOUS EMISSION [5][7]

An accelerated electron will radiate electromagnetic energy. The power radiated by a relativistic electron is given by the generalized Larmor formula or Liénard result. For an accelerating force perpendicular to the direction of electron motion, the total power radiated by a single electron is

$$P_e = \frac{2}{3}\frac{e^2\gamma^4}{c}\dot{\beta}_\perp^2 . \tag{2.8}$$

This power is distributed in space according to

$$\frac{dP_e}{d\Omega} = \frac{2e^2\gamma^6}{\pi c}\frac{\dot{\beta}_\perp^2}{(1+\gamma^2\theta^2)^3}\left[1 - \frac{4\gamma^2\theta^2\cos^2\phi}{(1+\gamma^2\theta^2)^2}\right] \tag{2.9}$$

where θ is the angular deviation from the longitudinal axis in the plane of acceleration, ϕ is the angular deviation from the longitudinal axis perpendicular to the plane of acceleration, and Ω is the solid angle into which the power is radiated. This power distribution is illustrated in Figure 3. The total power is radiated into a narrow cone of width, $\Delta\theta \approx 1/\gamma$ and solid angle $\Delta\Omega \approx 1/\gamma^2$ centered along the direction of motion. This narrow beam causes the optical radiation within the FEL laser cavity to have an intense energy density complicating FEL resonator designs due to the limitations of the optical components.

Photons emitted from the electron will have an energy, $E = hc/\lambda$, where λ is given by the resonance condition. Therefore,

$$E = \frac{2hck_o\gamma^2}{(1+K^2)} \tag{2.10}$$

where k_o is the wavenumber associated with the undulator static magnetic field. The time the electron spends within the undulator interaction region is $\Delta t = L/c$, where L is the total length of the undulator. The number of photons emitted per electron in one pass of the undulator, then, can be easily determined by multiplying the total power emitted from an electron, equation 2.8, by Δt and then dividing by the energy per photon, equation 2.10. In the next section we will see that $\dot{\beta}_\perp^2 = K^2k_o^2c^2/\gamma^2$ so that the number of photons spontaneously emitted per pass, W_e, is

$$W_e = \frac{2\pi}{3}N\alpha K^2(1+K^2) \approx 2N\alpha K^2 \tag{2.11}$$

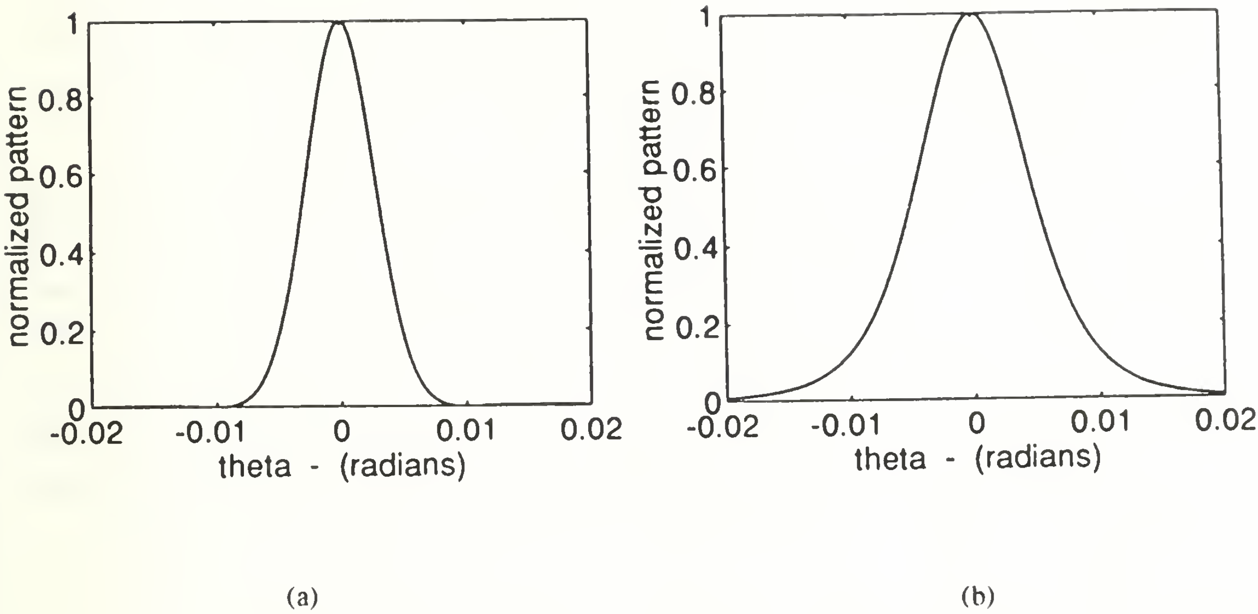

Figure 3 - Radiation pattern from a relativistic electron ($\gamma = 100$) under a transverse acceleration, (a) $\phi = 0$, (b) $\phi = \pi/2$

where $\alpha = e^2/\hbar c \approx 1/137$ is the fine structure constant and $N = L/\lambda_o$ is the total number of undulator periods. For an undulator design with $K \approx 1$ and $N = 100$, about three photons will be emitted per electron per pass through the undulator. Not all of these photons, however are emitted into the coherent optical mode. The coherent optical mode size is controlled by the Rayleigh length, z_o, which is the propagation distance required for the optical mode cross-sectional area to double. The number of photons emitted into the solid angle $\Delta\Omega \approx 1/N\gamma^2$ defined by the coherent optical mode with a Rayleigh length comparable to the length of the undulator [5] is

$$W_c = \frac{\pi}{3}\,\alpha K^2\,(1+K^2) \approx \alpha K^2 \tag{2.12}$$

Therefore, only about 1% of the electrons will spontaneously emit a photon into the coherent optical mode per pass.

The above relations imply two significant factors. First, the total photon energy emissions are many orders of magnitude less than the total electron energy so that momentum recoil imparted to the electron has a negligible effect on the electron's trajectory. Secondly, the process of spontaneous emission constitutes the initial mechanism for FEL startup only. The primary power transfer mechanism from the electrons to the optical fields after a small power density has built up within the laser resonator cavity is stimulated emission. At saturation, up to a few percent of the electron beam energy may be extracted per pass of a micropulse through the undulator by stimulated emission.

The electron micropulses passing through the undulator create optical pulses of similar length. The expression for the resonance condition, equation 2.6, is derived based on the electron slipping one optical wavelength behind the photon every undulator wavelength. Therefore, we might expect that the minimum length of the optical pulse will be $N\lambda$. This length is called the "slippage distance" since the electron micropulse slips a total distance of $N\lambda$ along the optical pulse as the micropulse travels down the undulator. Actual optical pulses are often longer than the slippage distance, and under certain conditions, called "short pulse effects," may even be shorter than the slippage distance.

C. ELECTRON DYNAMICS AND THE PENDULUM EQUATION [5]

The energy transfer between the electron beam and the optical wave occurs in the interaction region of the undulator. Within this region, the electric field is due exclusively to the optical electromagnetic wave while the magnetic fields are due both to the optical wave and the static undulator magnetic field. The first FEL was developed with helically polarized undulator magnetic fields and has a simpler mathematical development for some FEL phenomena. Currently most FELs have linearly-polarized undulators. The fields within an undulator linearly polarized in the vertical ($\hat{y}$) direction are illustrated by Figure 4 and are given by

$$\vec{B}_m = B_o \sin(k_o z)\ \hat{y} \tag{2.13}$$

$$\vec{E}_r = E\ cos(kz - \omega t + \phi)\ \hat{x} \tag{2.14}$$

$$\vec{B}_r = E\ sin(kz - \omega t + \phi)\ \hat{y} \tag{2.15}$$

where $\omega = kc$ is the angular frequency of the optical radiation, the subscript "m" represents an undulator parameter and the subscript "r" represents an optical wave parameter.

In order to describe the electron dynamics and trajectories, we return to the Lorentz equations as applied to a linearly polarized undulator.

$$\frac{d}{dt}(\gamma \vec{\beta}) = -\frac{e}{mc}\left[\vec{E}_r + \vec{\beta} \times (\vec{B}_r + \vec{B}_m)\right] \tag{2.16}$$

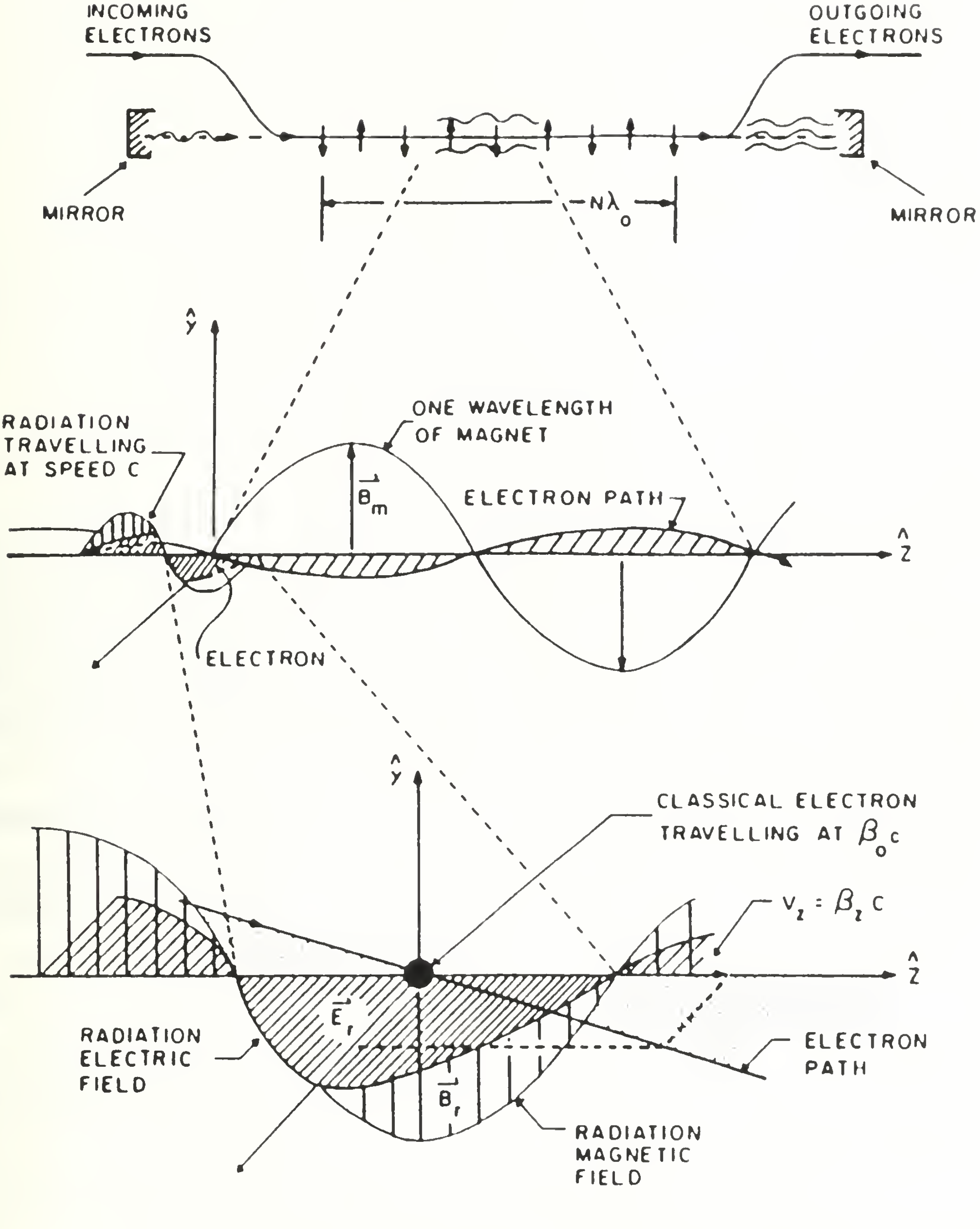

Figure 4 - Fundamental physics of the FEL interaction. After Ref. [4]

$$\frac{d\gamma}{dt} = -\frac{e}{mc}\left[\vec{\beta} \cdot \vec{E}_r\right] \tag{2.17}$$

$$\gamma = \frac{1}{\sqrt{1 - \vec{\beta} \cdot \vec{\beta}}} \tag{2.18}$$

Equations 2.16 and 2.18 combine to obtain

$$\beta_\perp = -\frac{\sqrt{2}K}{\gamma} \cos(k_o z) \tag{2.19}$$

$$K = \frac{e\bar{B}_o \lambda_o}{2\pi mc^2} \tag{2.20}$$

$$\beta_z = \sqrt{1 - [1 + K^2(1 + \cos(2k_o z)] / \gamma^2} \tag{2.21}$$

and substituting equation 2.19 into equation 2.17 we obtain

$$\frac{d\gamma}{dt} = \sqrt{2}\,\frac{eEK}{\gamma mc}\, cos\,(kz - \omega t + \phi) \tag{2.22}$$

Integrating equation 2.19 and plugging in representative values for existing FELs [5], we find that the transverse deflection of the electron beam as it passes through the undulator is on the order of 0.2 mm. Furthermore, undulator wavelength values are on the order of 5 cm. Therefore, even with $N = 100$ periods for the undulator, the undulator is only a few meters long. The laser resonator, however, may be much longer to allow the optical beam size to increase and reduce the power density impacting on the mirrors.

The electron trajectories described by the above equations have oscillatory components within an undulator wavelength. Over an undulator period, however, the electrons have an apparent average or constant trajectory. It is convenient to define the electron's position in terms of the electron phase, ζ, as

$$\zeta = (k + k_o)\bar{z} - \omega t \tag{2.23}$$

where $\bar{z}$ is the position of the electron given its average motion neglecting the oscillations. Since $k \gg k_o$, $\Delta\zeta \approx k\,\Delta\bar{z}$. A change $\Delta\bar{z} \approx \lambda$ corresponds to a $\Delta\zeta \approx 2\pi$ radians. From equation 2.21, we obtain

$$\bar{\beta}_z = \sqrt{1 - \frac{1 + K^2}{\gamma^2}} \tag{2.24}$$

and

$$z = \bar{z} - \frac{\xi}{k} \sin(2k_o ct) \tag{2.25}$$

where $\xi = K^2/2(1+K^2)$ and $k_o z \approx k_o ct$ since the electrons are traveling at nearly the speed of light. Substituting equations 2.23 and 2.25 into equation 2.22 we obtain

$$\frac{d\gamma}{dt} = \frac{eEK}{\sqrt{2}\,\gamma mc}\left\{\cos[(\zeta+\phi)-\xi\sin(2k_o ct)]+\cos[(\zeta+\phi)-2k_o ct-\xi\sin(2k_o ct)]\right\}. \tag{2.26}$$

Averaging equation 2.26 over one undulator period results in

$$\overline{\frac{d\gamma}{dt}} = \frac{eEK\,[J_o(\xi)-J_1(\xi)]}{\sqrt{2}\,\gamma mc}\,cos(\zeta+\phi) \tag{2.27}$$

Differentiating equation 2.23 with respect to time twice and equation 2.24 once, they combine with the resonance condition and simplify to give

$$\frac{d^2\zeta}{dt^2} = \frac{\sqrt{2}\,k_o eEK_L(\xi)}{\gamma^2 m}\cos(\zeta+\phi) \tag{2.28}$$

where $K_L(\xi) = K\,[J_o(\xi)-J_1(\xi)]$. Equation 2.28 is called the FEL pendulum equation.

The pendulum equation describes an important physical phenomena in FELs called "electron bunching". This is easily seen in equation 2.27. Consider a group of electrons uniformly distributed over a $\Delta\zeta \approx 2\pi$ space. Those electrons in the vicinity of $\zeta+\phi \approx \pi$ will experience a loss in energy and slow down. Those electrons near $\zeta+\phi \approx 0$ will gain energy and speed up. Therefore, the electrons will tend to bunch together near $\zeta = \pi/2$. Notice that the electron bunching is periodic over a $\Delta\zeta = 2\pi$ corresponding to $\Delta z \approx \lambda$. The coupling between the pendulum equation and the wave equation allows for the net transfer of energy from a bunched electron beam.

D. THE FEL SELF-CONSISTENT WAVE EQUATION [5][8]

The propagation of the optical wave is governed by the wave equation. The form of the wave equation applicable in the undulator interaction area is

$$\left[\nabla^2 - \frac{1}{c^2}\frac{\partial^2}{\partial t^2}\right]\vec{A} = -\frac{4\pi}{c}\vec{J}_\perp \tag{2.29}$$

where $\vec{A}$ is the vector potential and $\vec{J}_\perp$ is the transverse electron beam current. For an electron beam and optical wave in the interaction region of a linearly polarized undulator

$$\vec{A} = \frac{E(z,t)}{k}\,sin(kz-\omega t+\phi)\;\hat{x} \tag{2.30}$$

$$\vec{J}_{\perp i} = -ec\vec{\beta}_\perp\,\delta^3(\vec{x}-\vec{r}_i)\;\hat{x} \tag{2.31}$$

$$\vec{\beta}_\perp = -\frac{\sqrt{2}\,K}{\gamma}\, cos(k_o z)\ \hat{x} \tag{2.32}$$

where $\delta^3(x)$ is the three-dimensional delta function and the subscript "i" represents values of the i^{th} electron such that $\vec{J} = 0$ except at the exact location of an electron. The transverse beam current is a summation of the contributions of individual electrons.

Substituting equation 2.30 into equation 2.29 results in a complex expression. Since we are using the FEL to produce coherent, monochromatic light, we can apply the slowly-varying amplitude and phase approximation,

$$\frac{\partial E}{\partial z} \ll k\,E\,, \qquad \frac{\partial E}{\partial t} \ll \omega\,E\,,$$

$$\frac{\partial \phi}{\partial z} \ll k\,\phi\,, \qquad \frac{\partial \phi}{\partial t} \ll \omega\,\phi\,. \tag{2.33}$$

This approximation is useful for coherent monochromatic sources because the inverse Fourier transform of a narrowband signal corresponds to a slowly-varying envelope on the optical wave. This approximation simplifies the second-order wave equation to the first-order equation

$$\left[\frac{\partial E}{\partial z}+\frac{1}{c}\frac{\partial E}{\partial t}\right]\cos(kz-\omega t+\phi)-E\left[\frac{\partial \phi}{\partial z}+\frac{1}{c}\frac{\partial \phi}{\partial t}\right]\sin(kz-\omega t+\phi) = -\frac{2\pi}{c}J_\perp\ \hat{x}\ . \tag{2.34}$$

Substituting in the expression for the electron beam current and averaging over a volume of the electron beam that is many optical wavelengths long, 2.34 simplifies to

$$\left[\frac{\partial}{\partial z}+\frac{1}{c}\frac{\partial}{\partial t}\right] Ee^{i\phi} = -2\sqrt{2}e\,\pi K\ \sum_i \left[\frac{\overline{e^{-i[(k+k_o)z-\omega t]}+e^{-i[(k-k_o)z-\omega t]}}}{\gamma_i}\right]\delta^3(\bar{x}-r_i) \tag{2.35}$$

where $[\ \overline{\dots}\ ]$ represents the average over many optical wavelengths. Using equations 2.23 and 2.25 we note that $(k+k_o)z-\omega t=\zeta-\xi\sin(2k_o z)$ and $(k-k_o)z-\omega t=\zeta-2k_o z-\xi\sin(2k_o z)$. Computing the average in equation 2.35, the wave equation is now

$$\left[\frac{\partial}{\partial z}+\frac{1}{c}\frac{\partial}{\partial t}\right] Ee^{i\phi} = -2\sqrt{2}\pi e K_L(\xi)\ \sum_i \frac{e^{i\zeta}}{\gamma_i}\ \delta^3(\bar{x}-\vec{r}_i)\ . \tag{2.36}$$

An electron beam consists of a large number of electrons making the calculation of the summation in 2.36 prohibitive. However, we can take a "few" electrons over an optical wavelength representative of the entire electron beam within that wavelength and compute the summation. Therefore, the FEL wave equation is

$$\left[\frac{\partial}{\partial z}+\frac{1}{c}\frac{\partial}{\partial t}\right] Ee^{i\phi} = -2\sqrt{2}\pi e K_L(\xi)\ \ < \rho(z)e^{-i\zeta}\,/\,\gamma >_{z=z-\bar{\beta}_z ct} \tag{2.37}$$

where ρ is the electron density and $< ... > = \frac{1}{\rho}\sum_{i=1}^{\rho}(...)$.

The wave equation and the pendulum equation are the two important equations describing the electron beam and optical wave interactions. However, it is more convenient to non-dimensionalize these equations for FEL analysis.

E. NON-DIMENSIONAL ANALYSIS AND PHASE-SPACE [5]

The pendulum equation, 2.28, and the wave equation, 2.37, are the principal equations of motion describing the electron beam and optical wave dynamics within an FEL. In most instances, it is necessary to analyze FEL properties numerically. Numerical analysis is simpler and results more physically meaningful when these equations are used in a non-dimensional form.

A convenient choice for non-dimensionalizing the FEL equations is to establish a coordinate system by normalizing time to the time it takes the optical wave (or electron beam) to traverse the length of the undulator and to reference distance according to the position of a point traveling at the speed of light. The transformations are $\tau = c/L\ t$ and $\tilde{z} = z - c\ t$, where τ is the non-dimensional time and $\tilde{z}$ is the position with respect to the reference position. The coordinate $\tilde{z}$ stays with a point on the field envelope traveling at speed c. For the special case where the electron pulse is many optical wavelengths long so that $\rho(z) = \rho$ and the electrons have a uniform and constant energy, then the non-dimensional pendulum equation and wave equation become

$$\frac{\partial^2\zeta}{\partial\tau^2} = \overset{\circ\circ}{\zeta} = \frac{2\sqrt{2}\pi LNeEK_L(\xi)}{\gamma^2 mc^2}\ cos(\zeta+\phi) \tag{2.38}$$

$$\frac{1}{L}\frac{\partial}{\partial\tau}(Ee^{i\phi}) = 2\sqrt{2}\pi eK_L(\xi)\frac{\rho}{\gamma}\ < e^{-i\zeta} > \tag{2.39}$$

Introducing the complex optical field envelope $a = |a|\ e^{i\phi}$, and the dimensionless current, j, where $|a| = 2\sqrt{2}\pi LNeEK_L(\xi)/\gamma^2 mc^2$ and $j = 8\rho N[e\pi LK_L(\xi)]^2/\gamma^3 mc^2$, the non-dimensional pendulum equation and wave equation are

$$\overset{\circ\circ}{\zeta} = |a|\ \cos(\zeta+\phi) \tag{2.40}$$

$$\overset{\circ}{a} = -j < e^{-i\zeta} > . \tag{2.41}$$

Typically, the optical mode waist (radius), $w_o = \sqrt{\lambda z_o/\pi}$, within the undulator is larger than the radius of the electron beam. Therefore, only part of the optical wave is amplified by the electrons. This is compensated for by including the "filling factor," $F = (r_b/w_o)^2$, in the dimensionless current, $j \rightarrow jF$.

The optical wave and electron evolution within the electron beam are coupled according to equations 2.40 and 2.41. The electron phase, ζ, represents the electron position within the electron pulse and the change in electron phase, $\Delta\zeta \approx k\Delta z$, is indicative of the change in electron position. The electron phase is periodic over a distance corresponding to one optical wavelength. Therefore, if we analyze the ζ evolution over a length of one optical wavelength (2π radians in phase) of the electron beam, then we know the ζ evolution over the entire electron pulse. It is convenient to select the ζ reference so that $\phi = 0$.

Another important parameter in our analysis of electron evolution is the phase velocity, $\nu = \overset{\circ}{\zeta} = L[(k + k_o)\bar{\beta}_z - k]$. Differentiating equation 2.24 and non-dimensionalizing we find that $\Delta\nu = 4\pi N\Delta\gamma/\gamma$. Therefore, the phase velocity is indicative of the electron energy and the change in phase velocity is indicative of the change in electron energy. A phase velocity of $\nu = 0$ corresponds to an electron exactly on resonance, whereas an electron with a $\nu = \pi$ will advance about $\lambda/2$ ahead of an electron on resonance over the length of the undulator.

The FEL phase space evolution depicted in Figure 5 shows an example of the change in electron energy and position for an initial uniformly distributed monoenergetic electron beam. If we can form electron bunching around $\zeta = \pi$, then a net amount of energy will be transferred from the electron beam to the optical field. An electron bunch centered around $\zeta = 0$, however, will cause a net energy to be absorbed by the beam from the field. Figure 5 shows the phase space evolution of a resonant electron beam, and a beam slightly above resonance. A resonant electron beam has no gain. This is because for a uniformly distributed electron beam at resonance, every electron which contributes energy to the optical field is balanced by another electron which absorbs an equal amount of energy from the field. An electron slightly above resonance will contribute a net energy to the optical field. This will be explained more fully in the next section. Through the process of mode competition in the FEL, the optical wavelength will adjust itself so that the electron beam will be slightly above resonance.

The "football-shaped" curve in Figure 5 is called the separatrix. The separatrix curve is given by

$$\nu_s^2 = 2|a|\,[1 - \sin(\zeta_s + \phi)] \tag{2.42}$$

where the subscript "s" refers to the separatrix values. An electron orbit enclosed within the separatrix is a "closed" orbit. This is equivalent to a pendulum swinging side-to-side with

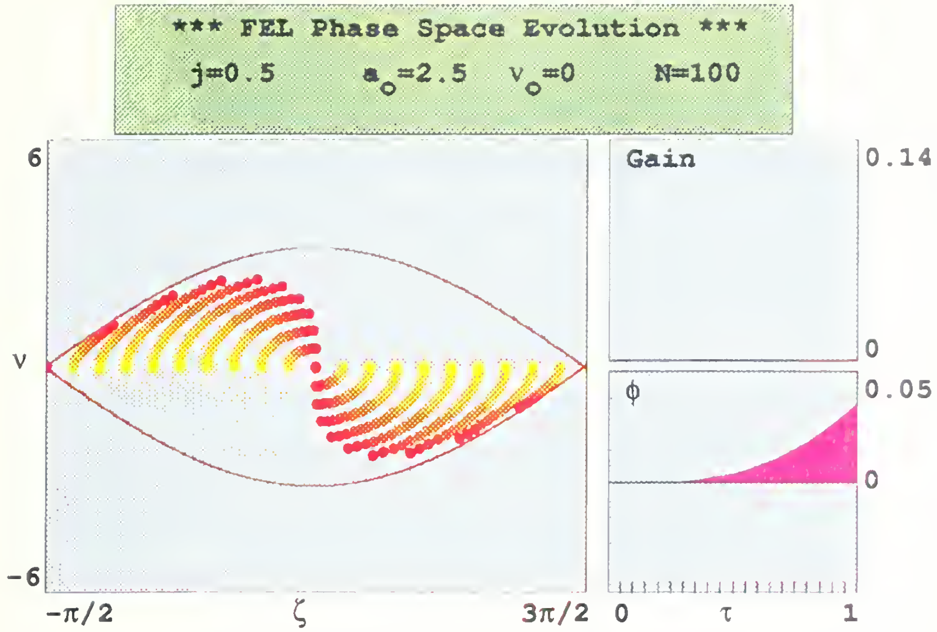

(a)

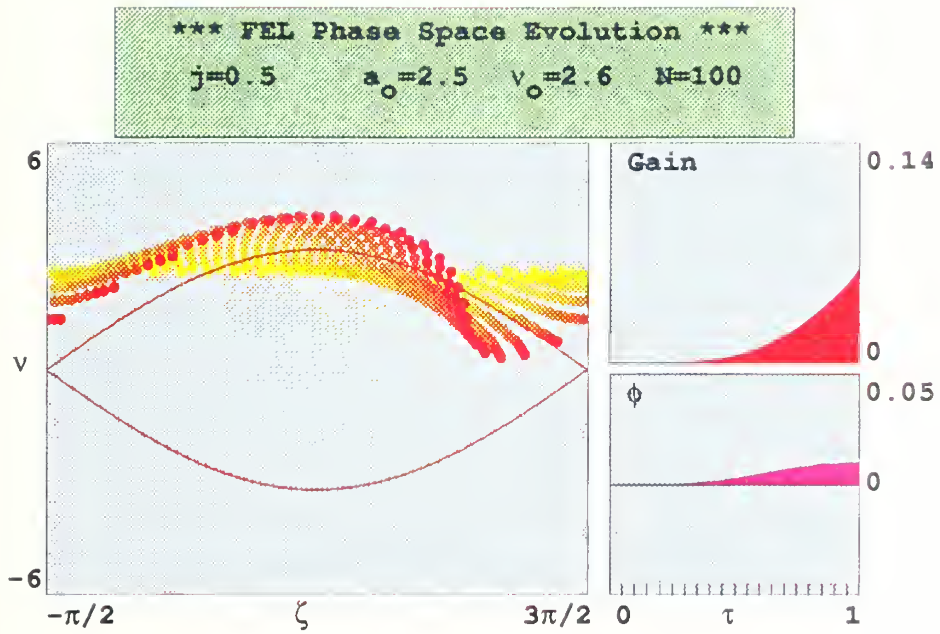

(b)

Figure 5 - Phase space evolution of an electron pulse, (a) resonance, (b) maximum gain

insufficient energy to reach the vertical position and "swing over the top". An electron orbit outside of the separatrix is an "open" orbit. Since these changes are periodic, an electron which leaves the field of $\Delta\zeta = 2\pi$ shown is replaced by another electron from an adjacent $\Delta\zeta = 2\pi$ section of the micropulse. This is equivalent to a pendulum swinging over the top on every revolution due to a total energy greater than that required to overcome the potential energy of the vertical position. In our FEL, however, energy is being transferred both to and from the electrons so they are not necessarily confined exclusively to one region or the other. As the complex field strength, $|a|$, increases, the separatrix becomes larger trapping a larger fraction of the electrons. For a maximum transfer of energy from the electron beam to the optical field, the electrons must bunch at $\zeta \approx \pi$ in the lower right-hand section of phase space enclosed within the separatrix.

F. WEAK OPTICAL FIELDS EVOLUTION [5]

From the pendulum and wave equations, it is clear that electron bunching around $\zeta+\phi \approx \pi$ provides for maximum gain of the optical fields. However, if the electron beam is over-bunched such that the bunch moves toward $\zeta+\phi \approx 0$ in phase space, then energy will be absorbed back into the electron beam. The weak-fields assumption, $|a| \lesssim \pi$, is defined such that the electron beam is not over-bunched. Over-bunching is indicative of strong optical field FEL interactions.

Under weak fields, we can expand the pendulum equation and wave equation to first order in $|a|$ and combine to form

$$\overset{\circ}{a} = \frac{ij}{2} \int_o^\tau \tau' \, F(\tau') \, |a(\tau-\tau')| \, e^{-i\nu_o\tau'} \, d\tau' \tag{2.43}$$

where

$$F(\tau') = \int_{-\infty}^{\infty} f(q) \, e^{-iq\tau'} \, dq. \tag{2.44}$$

Equation 2.43 is referred to as the <u>integral equation</u>. $F(\tau')$ is the characteristic function of the beam quality distribution $f(q)$. The initial phase velocities of the electrons are $\nu_i = \nu_o + q$ and are distributed about ν_o according to $f(q)$. For a perfect beam, where all of the electrons are injected monoenergetically with phase velocity ν_o into the undulator directly on axis with no transverse position or velocity components, then $F(\tau) = 1$.

The wave equation, 2.41, tells us that for low current conditions, $j \lesssim \pi$, the optical field does not change significantly per pass. Assuming perfect beam quality, the solution to the integral equation gives an optical field development per pass to first order in j,

$$a(\tau) = a_o \left\{ 1 + j \left[\frac{2 - 2\cos(\nu_o \tau) - \nu_o \tau \sin(\nu_o \tau)}{2\nu_o^3} \right] \right\} + \cdots \qquad (2.45)$$

and

$$\phi(\tau) = j \left[\frac{2\sin(\nu_o \tau) - \nu_o \tau (1 + \cos(\nu_o \tau))}{2\nu_o^3} \right] + \cdots , \qquad (2.46)$$

where a_o is the initial complex field strength. The gain of the optical field through the undulator in this low gain region is given by

$$G(\nu_o, \tau) = \frac{|a(\tau)|^2 - a_o^2}{a_o^2} \approx \frac{j}{\nu_o^3} \left[2 - 2\cos(\nu_o \tau) - \nu_o \tau \sin(\nu_o \tau) \right] . \qquad (2.47)$$

The weak fields, low current gain spectrum is shown in Figure 6.

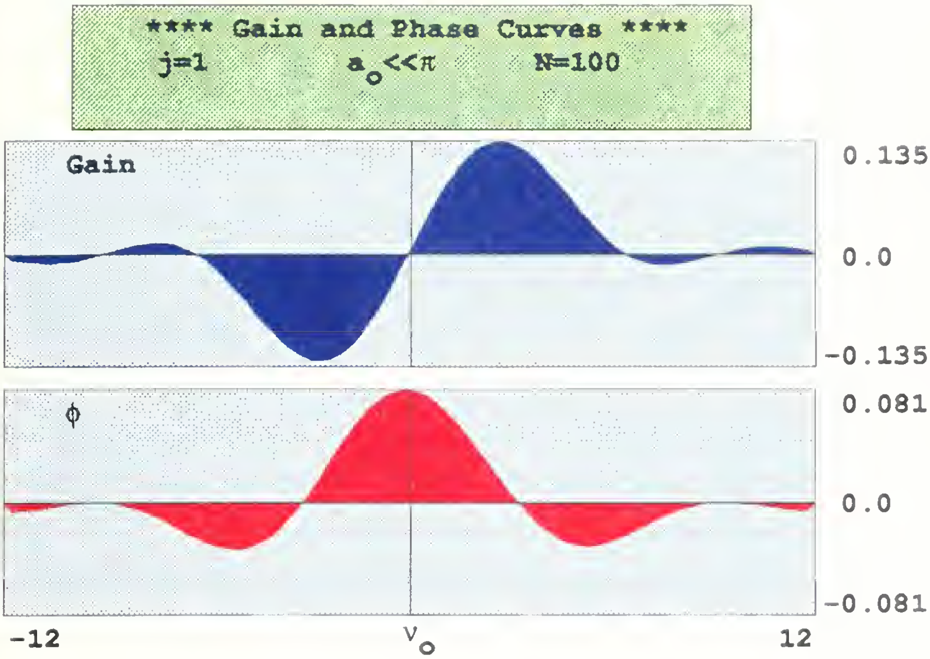

Figure 6 - Weak fields, low current anti-symmetric gain spectrum

The anti-symmetric gain curve shows several important FEL properties. First, there is no gain at resonance, $\nu_o = 0$. Secondly, the electron phase velocity must be slightly above resonance to achieve gain. The maximum gain is $G = 0.135j$ and occurs at an initial phase velocity $\nu_o = 2.6$.

Under high current, high gain conditions, $j >> \pi$, it can be seen from the wave equation, 2.41, that the magnitude of the optical field changes appreciably over a single pass. The self-consistent solution to the integral equation for this region provides much different results. Maintaining the assumption of perfect beam quality, an FEL operating on resonance, $\nu_o = 0$, will have a complex field development given by

$$|a(\tau)| \approx \frac{a_o}{3}\, e^{(j/2)^{1/3}\sqrt{3}\tau/2} \tag{2.48}$$

$$\phi(\tau) \approx \left(\frac{j}{2}\right)^{1/3} \frac{\tau}{2} \tag{2.49}$$

giving gain along the undulator of

$$G(\tau) \approx \frac{1}{9}\, e^{(j/2)^{1/3}\sqrt{3}\tau} \tag{2.50}$$

There is now gain for an electron beam directly on resonance. Off resonance, the single-pass gain at the end of the undulator is given by

$$G(\nu_o) \approx \frac{1}{9}\, e^{(j/2)^{1/3}\sqrt{3}\,(1\,-\,(\nu_o\tau_B/3)^2)} \tag{2.51}$$

where $\tau_B = (2/j)^{1/3}$ is the bunching time. The gain spectrum for the high gain region is shown in Figure 7. As in the low gain case, the peak gain is still slightly above resonance. The phase velocity that gives the peak gain, however, is now a function of current. As $j \rightarrow \infty$, the gain spectrum approaches a symmetric spectrum with the peak gain occuring at resonance.

The gain spectrum bandwidth can be determined from equation 2.51. Defining the bandwidth as the range of phase velocities where the growth rate is reduced by 10% [5], the bandwidth is $\Delta\nu_o \approx 2j^{1/3}$. Using this same definition, the gain bandwidth for the low gain case is about $\pi/2$. Therefore, the bandwidth for the high gain case is much larger than for the low gain case.

G. GAIN DEGRADATION DUE TO BEAM QUALITY [5]

The previous gain analysis assumed perfect beam quality. A real electron beam has an emittance, ε, where the electrons enter the undulator at an angle, θ_x, with respect to the undulator axis, or at a transverse position slightly off axis, x_o. The electrons will also have a small energy spread between them. The emittance and energy spread of the electron beam translates into a spread in phase velocities in phase-space. The phase velocity spread of an imperfect electron beam due to emittance is given by

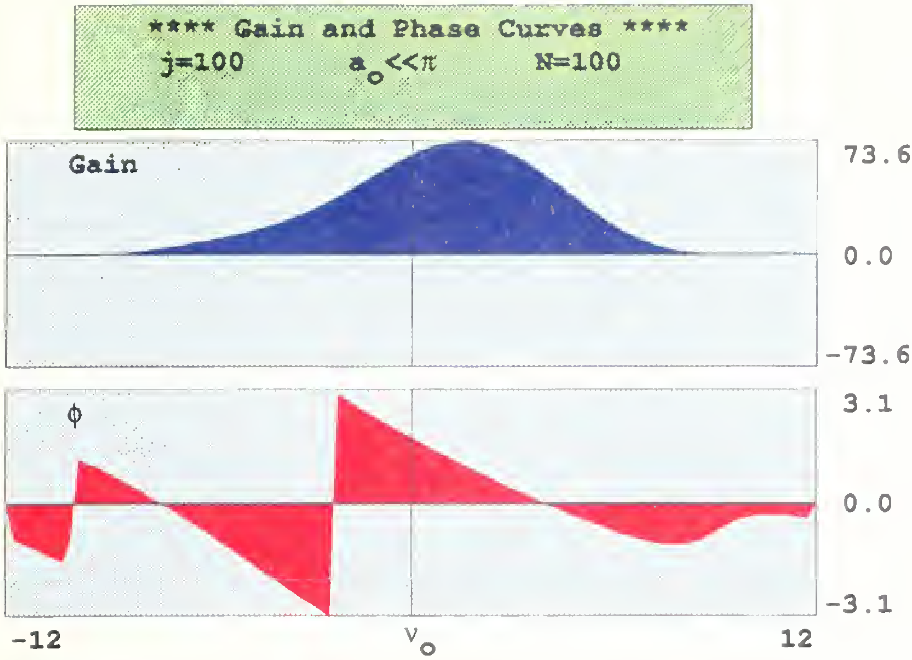

Figure 7 - Weak fields, high current gain spectrum

$$\Delta\nu \approx -\frac{2\pi N}{1+K^2}\,(K^2 k_o^2 x_o^2 + \gamma^2\theta_x^2). \qquad (2.52)$$

and the phase velocity spread due to energy spread is $\Delta\nu = 4\pi N\,\Delta\gamma/\gamma$.

Imperfect beam quality reduces the single-pass FEL gain by degrading electron bunching. Consider the integrand of the integral equation. The complex field strength grows as the electron beam travels down the undulator causing the integrand to increase. Therefore, the rate at which the optical field strength grows is faster. Equation 2.51 and a plot of equation 2.47 shows that this feedback causes exponential growth in the FEL optical field strength. With imperfect beam quality, however, the $F(\tau)$ decays over time so that this feedback mechanism is attenuated.

Electrons enter the undulator with a spread in phase velocities due to a spread in energies. Typical energy spreads from an accelerator are on the order of $\Delta\gamma/\gamma \approx 0.001$. The typical distribution of electron phase velocities is Gaussian about ν_o,

$$f_G(q) = \frac{e^{-q^2/2\sigma_G^2}}{\sqrt{2\pi}\,\sigma_G} \qquad (2.53)$$

where $\sigma_G = 4\pi N\,\Delta\gamma/\gamma$ is the standard deviation. The corresponding characteristic function is

$$F_G(\tau) = e^{-\sigma_G^2\tau^2/2}. \tag{2.54}$$

$F_G(\tau)$ decays over the length of the undulator with a time on the order of $1/\sigma_G$.

The change in phase velocity due to beam emittance has a quadratic dependence on electron position and entrance angle. Therefore, $f(q)$ is not the same as the distribution of x_o and θ_x. Electron pulses normally have a Gaussian distribution in space. A beam with matched contributions from position and angle, $\gamma\bar{\theta}_x = Kk_o\bar{x}_o$, where $\bar{\theta}_x$ and $\bar{x}_o$ are the rms deviations of the electron beam entrance angle and position, will have an exponential phase velocity distribution given by

$$f_\theta(q) = \frac{1}{\sigma_\theta}\, e^{q/\sigma_\theta} \qquad\qquad q \lesssim 0 \tag{2.55}$$

where $f_\theta(q) = 0$ for $q > 0$ and $\sigma_\theta = 4\pi N\gamma^2\bar{\theta}_x^2/(1+K^2)$. The corresponding characteristic function is

$$F_\theta(\tau) = \frac{1}{1 - i\sigma_\theta\tau}. \tag{2.56}$$

$F_\theta(\tau)$ decays over the length of the undulator with a time on the order of $1/\sigma_\theta$. A σ_θ or σ_G of about π will cause a random phase spread of about π.

The effect of beam quality on gain is illustrated in Figure 8 for the case of electron energy spread. At $\sigma_G = 0$, the gain spectrum is identical to Figure 6. As σ_G increases, however, the gain spectrum broadens, the phase velocity for peak gain increases, and most importantly the peak gain is reduced. Electron beam emittance has a similar effects.

H. STRONG OPTICAL FIELDS EVOLUTION AND SATURATION [5]

When an FEL reaches the strong field regime, the gain per pass is reduced. The FEL reaches saturation when the gain decreases to where it equals the optical resonator loss rate including the outcoupling of the mirrors. Strong fields can be detected in phase space by over-bunching of the electrons. This occurs when $|a| \gtrsim \pi$.

In strong fields, the separatrix now traps a significant amount of electrons in closed orbits. An electron bunch is quickly formed around $\zeta + \phi \approx \pi$ where these electrons amplify the optical wave. As the electrons lose energy, their phase slips towards the $\zeta + \phi \approx 0$ position and energy is absorbed back from the optical wave. This reduces the net gain per pass of the FEL.

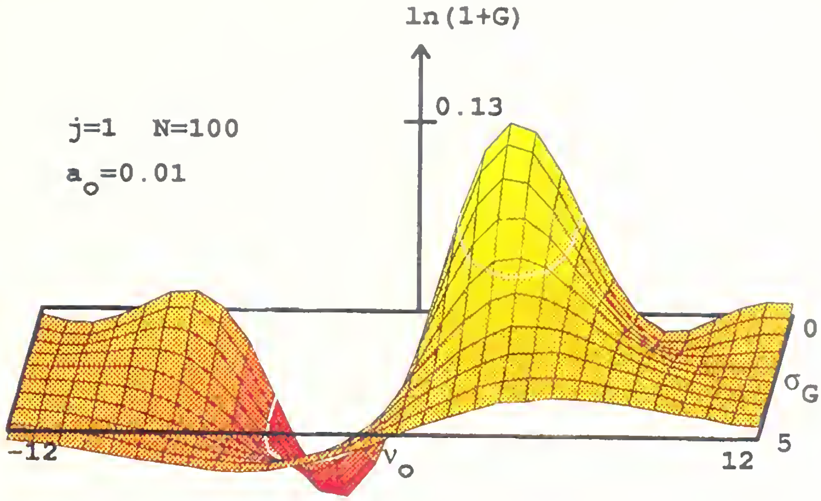

Figure 8 - Degradation of the weak fields, low current anti-symmetric gain spectrum due to electron beam energy spread

The gain degradation due to strong fields is illustrated in Figure 9. As the complex field strength and height of the separatrix increases, so does the gain degradation. Careful examination of Figure 9 reveals that strong-fields produce similar gain degradation characteristics as the energy spread effects of Figure 8. This is because the FEL interaction induces an energy spread among the electrons. Therefore, the gain is also reduced in a manner similar to a phase velocity spread of $\Delta\nu = 4\pi N\,\Delta\gamma/\gamma$. As the total energy loss of the electrons increases, a larger phase velocity spread is induced on the electrons. Eventually many electrons will move near the ends or even outside of the gain spectrum bandwidth reducing the gain of the optical fields. As the optical fields approach saturation, more total energy is still being removed from each passing micropulse, but the fractional increase in optical energy (gain) is being reduced.

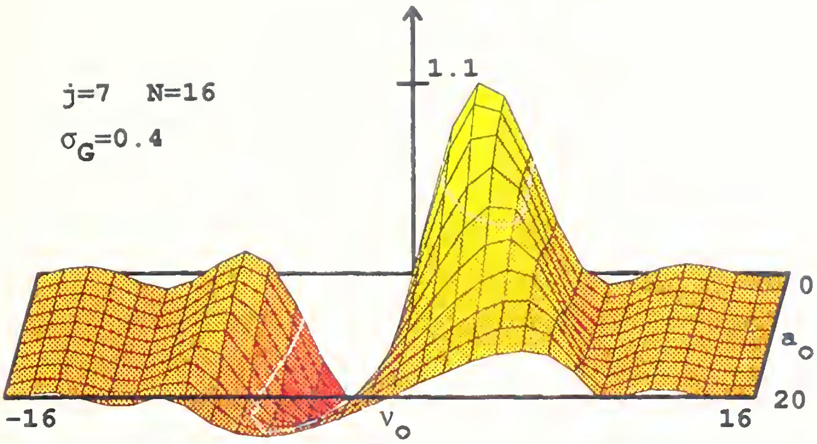

Figure 9 - Gain degradation due to strong optical fields

III. FEL SYSTEM POWER REQUIREMENTS

The principles of FEL operation outlined in the previous chapter describe how energy is extracted from a relativistic electron beam and radiated as coherent optical light. The production of a high quality relativistic electron beam, however, is a necessary engineering requirement. The basic functional components for a high-power FEL are the electron injector, the linear accelerator, the undulator and optical resonator, and the electron beam dump. Many technologies and configurations for each of these elements have been developed and applied. Existing FELs, however, operate at only a few watts of optical output and do not suffer from the infrastructure constraints of the naval shipboard environment including space availability, power generation and distribution, and adverse environmental conditions. In this chapter, the power requirements for a high-power FEL as applied to a potential shipboard weapons system are explored. All of the following technologies are currently in use or under development for FEL applications. Some of these technologies, however, will need further engineering development to support high-power operation.

A. SHIPBOARD ARCHITECTURE

In developing a shipboard high-power FEL, the issues that are of principal concern are system power efficiency, system size and weight, and personnel radiation hazards. The system size and weight are a direct function of beam energy, linear accelerator rf field frequency, system power efficiency, and optical resonator power density. Electron beam energy and the rf frequency determine the linear accelerator size and weight while the system power efficiency and the rf frequency determine the rf power source size and weight characteristics. Klystrons, klystrodes, and other high-power rf power sources suitable for accelerator applications contribute a significant fraction of the system size and weight. The optical resonator power density is much higher in an FEL than for a chemical or solid-state laser of equal energy storage due to the very small beam size. Therefore, FEL resonator length tends to be large in order to reduce the power density at the mirrors.

Of the existing or proposed, FEL architectures, only the energy recovery system depicted in Figure 10 optimizes all three concerns. In this scenario, electron pulses are injected into the accelerator at some small initial energy of approximately 4 MeV. The accelerator increases the beam energy by an order of magnitude or more. Bending magnets guide the beam and direct it into the undulator. The undulator will remove approximately 2 percent of the beam energy and convert it into optical energy. Additional bending magnets then guide the beam back into the

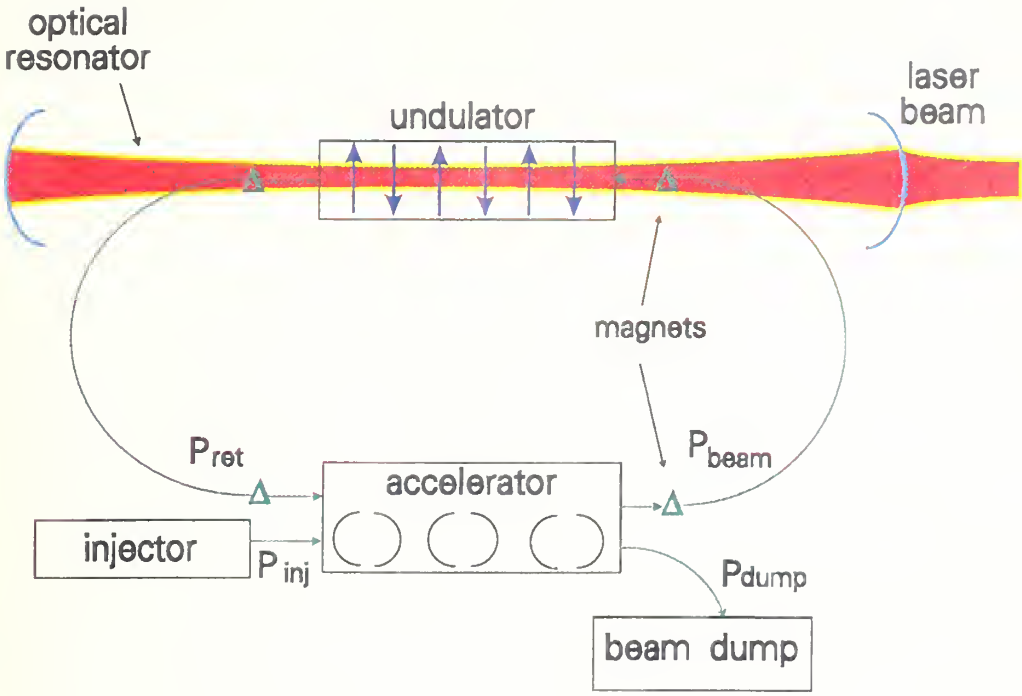

Figure 10 - Generic energy recovery FEL architecture

accelerator where it enters 180 degrees out of phase with the accelerating fields. The decelerating electron beam then transfers it's energy back into the rf fields. The energy recovered from the decelerated electron beam is then used to accelerate another electron pulse to repeat the cycle. The decelerated electron pulses are then directed into a beam dump where their residual energy is dissipated. This residual energy is about 5 MeV and is below the threshold of generating neutron radiation when it is dissipated in the beam dump.

This architecture is the most appropriate for several reasons. First, the energy efficiency is increased dramatically and the physical size of the system is reduced to that required in a shipboard environment. Most importantly, it is the only architecture which would reduce the personnel radiation hazards to manageable levels since there will be no neutrons and much lower energy gamma radiation. Table 1 is a listing of the neutron production threshold for several elements. These elements are commonly used as structural materials in shipboard applications or have significance with respect to neutron production in accelerator beam dumps. Only beryllium (Be) has a neutron production threshold below 5.9 MeV. Therefore, as long as

Element	Threshold (MeV)	Element	Threshold (MeV)	Element	Threshold (MeV)
Be	1.7	Cu	9.9	Mo	7.4
Os	5.9	Ni	11.4	Mn	10.2
*Li	7.3	Fe	11.2	Co	10.5
*C	18.7	Zn	10.2	Cr	12.0

Table 1 - neutron production thresholds [9]. All elements that have isotopes of $\gtrsim$ 10% abundance with thresholds below 6 MeV are included. * denotes elements with isotopes of less than 10% abundance with thresholds below 6 MeV

beryllium is excluded from the beam dump structural materials, neutron generation is not an issue. An architecture which does not utilize energy recovery will contain an inherent large radiation problem that will be much more difficult to solve due to the large radiation energies involved.

The feedback stability of this type of system has been numerically modeled and shown to be stable for several designs [10]. However, more comprehensive simulations, experiments, and possibly control systems engineering will be required to ensure stability at the higher currents examined in this thesis.

Since we are concerned with the FEL's potential as a naval laser weapon, the system must produce high output power at a wavelength suitable for propagation in a maritime atmospheric environment. The following power analysis will be developed for an FEL with a 1 MW optical output power at a wavelength of 3 μm. The FEL wavelength can be tuned over a range from this operating point so we will still have some flexibility in the actual operating wavelength. To establish the operational requirements, it is assumed that this laser will only need to operate for three shots of 15 second duration within one minute and ten shots over a twenty minute interval. This requirement has no basis in the time required to destroy a missile with a laser. Rather, it was chosen because a missile traveling at a speed of 0.9 Mach could be engaged over a closing distance of about 5 km.

To estimate the system power requirements, it is necessary to determine the electron beam energy and current. The resonance condition of equation 2.6 gives the required relationship between the electron beam energy, the undulator spatial wavelength, and the optical wavelength. For given undulator and optical wavelengths, the electron beam Lorentz factor must be

$$\gamma = \sqrt{\frac{(1 + K^2)\, \lambda_o}{2\, \lambda}} . \tag{3.1}$$

Current and planned FELs are summarized in Table 2 [11]. The undulator parameter, K, is typically on the order of unity so that $\gamma \approx \sqrt{\lambda_o / \lambda}$.

The power in an electron beam is the product of the electron beam energy, $W_b = \gamma mc^2$, and the average electron beam current, I_{avg}. For the architecture of Figure 10, only about 2 percent of the beam energy can be extracted by the undulator to allow for efficient energy recovery [3][12][13]. However, only a few experiments have been performed which demonstrate energy recovery but none of these have determined the accelerator energy recovery efficiency, η_{rec}, dependence on the undulator energy extraction efficiency, η_o. Therefore, the assumption that no more than 2% of the beam energy can be extracted within an energy recovery architecture may be conservative. Regardless of η_o, an electron beam cannot be decelerated much below 3 MeV because the electron velocity and rf phase velocity are no longer essentially the same. The maximum energy recovery efficiency is given by $\eta_{\max} = 1 - (3\text{ Mev})/W_b$. However, energy extraction in the wiggler introduces an energy (velocity) spread among the electrons in the beam which further reduces η_{rec}. More experiments are needed to determine the dependence of η_{rec} on η_o.

For a 1 MW optical output with η_o = 2%, 50 MW of electron beam power is required. In order to limit the undulator and optical resonator size and the required beam current, a maximum beam energy is desired. From equation 3.1, W_b = 100 MeV and I_{avg} = 500 mA are chosen as the design parameters for the production of 50 MW of beam power. For this beam energy, a η_{rec} = 95% is assumed.

It is desirable to maximize η_o so that the total electron beam power can be reduced. This will provide several advantages. First, by reducing the required I_{avg}, a high-power FEL is closer to realization. Current technologies can only expect to produce average currents of 10-100 mA [2][14]. Second, reducing W_b reduces the size, weight, and expense of the accelerator structures and allows for the production of longer wavelength light that may be more advantageous in a maritime environment.

FEL	λ (μm)	σ_z	E_a (MeV)	I (A)	N	λ_0 (cm)	K
EXISTING FELs:							
UCSB(mm FEL)	338	25μs	6	2	42	7.1	0.71
Stanford(FIRFEL)	80-200	15ps	4	8	50	1	0.7
UCSB(FIR FEL)	63	25μs	6	2	150	2.0	0.13
Tokyo(UT-FEL)	43	10ps	13	22	40	4	0.7
Holland(FELIX)	40	5ps	25	50	38	6.5	1.5
Osaka(ISIR)	40	30ps	17	50	32	6	1
Bruyeres(ELSA)	20	30ps	18	100	30	3.2	0.8
Frascati(LISA)	15	7ps	25	5	50	4.4	1
Grumman(CIRFEL)	14	5ps	14	150	73	1.36	0.2
Beijing(IHEP)	10	4ps	30	14	50	3	1
Orsay(CLIO)	8	0.3ps	50	80	48	4	1
LANL(AFEL)	4-6	10ps	15	200	24	1	0.27
Darmstadt(IR-FEL)	5	2ps	40	2.7	80	3.2	1
Stanford(SCAFEL)	5	0.7ps	37	10	72	3.1	0.83
Vanderbilt(FELI)	3	1ps	43	50	47	2.3	1
Duke(MarkIII)	3	3ps	44	20	47	2.3	1
BNL(ATF)	0.5	6ps	50	100	70	0.88	0.35
BNL(ATF-UV)	0.25	6ps	70	100	70	0.88	0.35
LANL(APEX)	0.37	10ps	46	135	73	1.36	0.58
Tsukuba(NIJI-IV)	0.35	160ps	300	5	2x42	7.2	2
Orsay(Super-ACO)	0.35	250ps	800	.1	2X10	13	4
Okazaki(UVSOR)	0.3	6ps	500	5	2x8	11	2
Novosibirsk(VEPP)	0.24	35ps	350	6	2x33	10	1.6
PROPOSED FELs:							
Florida(CREOL)	231-600	CW	1.7	0.2	185	0.8	.15
Netherlands(TEUFEL)	180	20ps	6	350	50	2.5	1
Rutgers(IRFEL)	140	25ps	38	1.4	50	20	1
Moscow(Lebedev)	100	20ps	30	0.25	35	3.2	0.75
Tokai(SCARLET)	40	40ps	15	10	62	3.3	1
Stanford(FIREFLY)	40	2ps	20	6	25	6	1
LBL(IRFEL)	3-50	33ps	55	60	40	5	1
CEBAF(IRFEL)	2-24	2ps	50	100	25	6	3.1
Boeing(APLE)	10	60ps	17	140	101	2.4	0.2
Boeing(APLE)	10	18ps	34	450	257	3.9	1.2
Stanford(FEL)	10	4ps	24	25	52	2.6	0.87
Osaka(ILT)	10	2ps	9	100	30	.66	0.3
UCLA(IRFEL)	10	2ps	20	200	40	1.5	1
Novosibirsk(RTM)	7	50ps	51	100	4x40	9	1-2
BNL(HGHG)	3.35	10ps	30	110	83	1.8	1.4
CEBAF(UVFEL)	0.15-2	0.4ps	200	200	48	3	1.5
Osaka(FELI)	1	2ps	170	100	50	6	1.26
Rocketdyne	0.84	3ps	90	500	160	2.4	1.4
Dortmund(DELTA)	0.4	50ps	500	90	17	25	3.1
ENEA-Frascati	0.2-0.3	15ps	2.3	4	8	2.5	1
Harima(HIT)	0.28	100ps	500	3	170	1.8	4.2
BNL(DUVFEL)	0.075	6ps	310	300	682	2.2	1.54
Duke(Ring)	0.05	10ps	1000	350	2x33	10	1.7
SLAC(LCLS)	0.0004	0.1ps	7000	2500	723	8.3	4.4

Table 2 - Summary of existing and proposed FELs [11]

B. ACCELERATOR STRUCTURE

A typical linear accelerator is comprised of a number of rf cavity cells like those depicted in Figure 11.

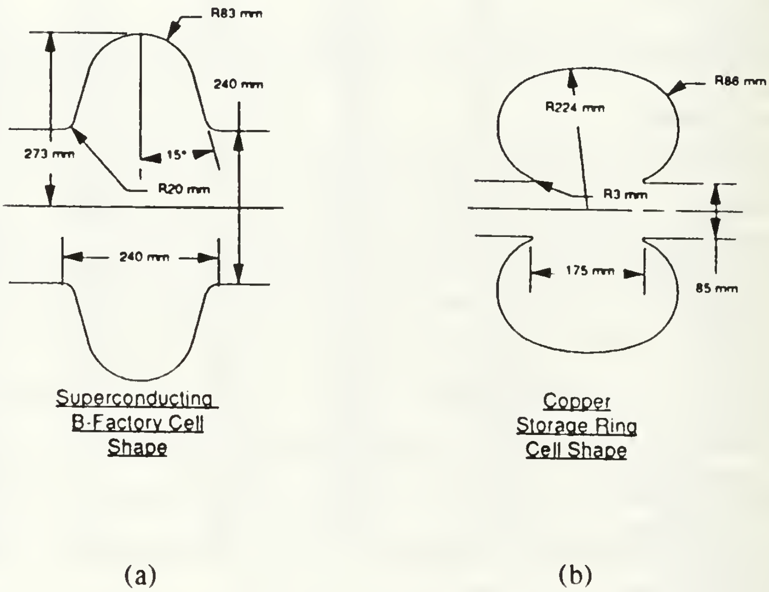

Figure 11 - Typical accelerator cells, (a) superconducting (b) room temperature. From Ref. [15]

Linear accelerator structures are fabricated from both room temperature (RT) and superconducting (SC) materials. SC structures reduce operating power requirements due to the low ohmic losses in the accelerating cavity walls. They also have higher allowed operating fields and accelerating gradients as well as much larger apertures between cells in the cavities. An accelerating electron forms an image charge within the accelerator structure. As it passes through an aperture connecting two cells, the image charge is now much closer to the electron beam axis. These image charges have a disruptive effect on the beam quality. The larger apertures mean that image charges will have a lesser disruptive effect in SC structures than RT structures. The higher gradients mean that SC structures can accelerate the electron beam to the desired W_b over shorter accelerator lengths than RT structures reducing the total weight and volume of the structure. RT structures, however, are forced to have geometries that intensify the harmful beam quality effects in an effort to minimize power dissipation [16]. RT structures still have applications because they are less expensive and easier to fabricate than the

SC structures and they don't require a large and inefficient liquid helium refrigeration system.

The development, theory, and design behind accelerators is complicated and requires extensive numerical modeling. In performing a power requirements analysis, however, accelerating cavities can be characterized by a few parameters for most purposes [16][17][18]. The significant parameters are the rf frequency, f (MHz), the cavity quality factor, Q, the shunt impedance, $Z = R_{sh}/Q$ (Ω/m) where R_{sh} is the shunt resistance, the cavity active length, L_a (m), and the average acceleration gradient, E_a (MV/m). The power dissipated per unit length is

$$P = \frac{E_a^2}{Z\ Q} \tag{3.2}$$

RT cavities typically have a $Q \approx 2\times10^4$ and an $E_a \approx 2$ MV/m compared to values for SC cavities of 3×10^9 and 10 MV/m respectively. Some actual values are shown in Table 3. The dissipated power is supplied to the accelerator by the rf power source.

cavity	f (MHz)	E_a (MV/m)	Q	Z (Ω/m)
TESLA (SC) [19]	1300	20	$>5\times10^9$	1100
CEBAF (SC) [2]	1500	8	5×10^9	1020
CDRL (SC)* [20]	500	5.3	2×10^9	400
TEUFEL (RT) [21]	1300	2	18330	1714

Table 3 - Typical cavity parameters (* - parameters from a proposal)

In order to properly apply equation 3.2, it is necessary to more fully characterize the parameters. Superconductivity is characterized by the BCS (Bardeen, Cooper, and Schrieffer) theory. For a SC cavity, the surface resistance, $R_s = R_{BCS} + R_{res}$, is given by the relation [16][17]

$$R_s = A\ \frac{f^2}{T}\ e^{-\frac{\Delta(T)}{2k_B T}} + R_{res} \tag{3.3}$$

where A ($\Omega\cdot$K/m/MHz^2) is the BCS material-dependent constant, Δ (eV) is the energy gap of the SC material used to form Cooper pairs, T (K) is the absolute temperature of the SC structure, k_B (eV/K) is the Boltzmann constant, and R_{res} (Ω/m) is the residual losses of the SC structure after fabrication ($R_{res} \approx 1-10\ \mathrm{n}\Omega/\mathrm{m}$). The quality factor of an accelerator cavity is the ratio of the energy stored within the cavity to the rf energy dissipation within the cavity per rf cycle. The Q value is related to the surface resistance through a geometry factor, G, by

$$Q = \frac{G}{R_s}, \qquad \frac{1}{Q} = \frac{1}{Q_{BCS}} + \frac{1}{Q_{res}} \tag{3.4}$$

where Q_{BCS} is the contribution to the quality factor due to losses in the superconductor and Q_{res} is the residual losses contribution to the quality factor. The geometry factor varies from 270 to 290 ohms [17]. An average value of $G = 280\ \Omega$ is assumed. With proper fabrication and conditioning techniques, a Q_{res}, of better than 5×10^9 can be obtained [16][17].

The shunt impedance is also a function of frequency. In the absence of other changes, the shunt impedance is proportional to frequency [22]. However, as the frequency changes, the subsequent scaling of the cavity dimensions allow us to make more favorable, slight adjustments in cavity geometry. A curve fit to existing SC cavities is [17]

$$Z = 380\,(f/500)^{.9} \qquad (\Omega/\mathrm{m})\,. \tag{3.5}$$

The cavity geometry changes do not have a very large effect on the shunt impedance. This is due to characteristics of SC cavities like the very large apertures which can be seen in Figure 11. As a result, the variations are incorporated into the frequency scaling of equation 3.5 instead of the geometry factor.

SC cavities are currently made exclusively of niobium (Nb). Although there are many SC materials available, it is desirable to use a material with the highest superconducting critical temperature, (T_c), and that can support the highest rf field strength, (H_c), without forcing it out of its superconducting state. It must also have a widespread availability, relative ease of fabrication, high thermal conductivity to dissipate heat, significant material phase stability, and have stable superconducting properties. Only lead (Pb) and Nb currently meet these requirements with Nb having the larger values of T_c and H_c. High temperature superconductors are currently unsuitable for these applications because of large surface resistances ($R_s \gtrsim 10^{-5}\Omega$) and low H_c (the highest values are 1/16 that of Nb) [16].

The BCS material constant for Nb is $A = .000028/(500)^2$. The static heat load of a SC cavity due to power couplers, etc. is typically about 8 W/m at 500 MHz [17]. Therefore, the total power dissipated in the cavity is $P_L = P_{static} + P_{BCS} + P_{res}$, that is

$$P_L = \frac{8}{\sqrt{f/500}} + \frac{E_a^2}{380\,(f/900)^{.9} Q_{res}} + \frac{E_a^2 (f/500)^{1.1} (.000028) e^{-17.67/T}}{380(280)T} \quad (\mathrm{W/m})\,. \tag{3.6}$$

RT cavities, normally fabricated from copper, have a surface resistance which is proportional to the square root of the frequency and the cavity Q is inversely proportional to the square root of the frequency for a fixed geometry [22][23]. Therefore,

$$P_L = \frac{E_a W}{k_1 \sqrt{f}} \tag{3.7}$$

and

$$Q = \frac{k_2}{\sqrt{f}}\,, \tag{3.8}$$

where k_1 and k_2 are geometry constants that are inversely proportional to the square root of both the electrical resistivity and magnetic permeability of the cavity material. The shunt impedance, then, is proportional to frequency and independent of the material from which the cavity is fabricated or its surface finish [22]. The constants, however, are heavily dependent on cavity geometry. Unlike with SC structures, the geometry constants vary widely with the rf frequency as adjustments to cavity geometry are made with the scaling of the cavity dimensions. This is apparent from Figure 11 with the RT cavity cell's narrow apertures. The values of k_1 for existing designs vary over the range $0.9 < k_1 < 4$ (Ω/m/MHz$^{1/2}$) [12][20][21][23]. Lower frequency cavities will have larger values of k_1.

The electron beam is a series of micropulses that are separated in space by some integer number of rf wavelengths, λ_{rf}. These micropulses can either be injected into the accelerator in macropulses or in CW mode. For a high-power FEL, CW mode is preferred [13] because:

1. The peak power of a micropulse is reduced. In reducing the total charge contained within a micropulse, it is easier to overcome the disruptive space charge effects that degrade the electron beam quality. Furthermore, the problem of electron beam "halo" is reduced. A real electron beam has a transverse spatial distribution. Although the electron density away from the beam transport axis is a small fraction of that on axis, the number of these electrons in a high current pulse is significant. These electrons can strike the magnetic beam transport optics and deflect so that they excite rf modes and cause transport instabilities for the entire beam. Similarly, the activation of the optics would create a significant radiation hazard over a very short time [12][14].

2. The peak power of the optical pulses developed in the optical resonator is reduced extending the lifetime of the mirrors and various optical components. Furthermore, the more constant loading of the optics reduces the need for stabilization measures due to transient deformations.

3. The overall power efficiency of the accelerator is increased. When electron pulses are accelerated in macropulses, the rf power is applied to the accelerator in pulses (pulsed power operation). A finite "filling time" is required to build up the energy storage within the accelerator cavity prior to the injection of the next macropulse. There is significant energy lost in the accelerator during both this filling time and the decay time at the end of the macropulse where stored energy within the cavity is dissipated.

4. Optimization of an energy recovery system is possible. Pulsed power systems have significant time variations of the electron beam parameters over the duration of the macropulse. This affects the optical evolution in the resonator. In CW mode, these variations occur over only a small fraction of the electron beam's duration and are not repetitive.

5. Finally, the control systems are easier to realize. They can be simpler, slower, and much less expensive than for an equivalent pulsed power machine. This is an extremely important factor because the feedback and control requirements for a high-average power energy recovery system are formidable. Studies into the control system requirements for these systems are just beginning [10][12].

The final consideration in determining the power requirements is in the choice of rf frequency. In general, it is preferred to have as low a frequency as possible without the size and capital cost of the accelerator structure becoming excessive. Lower frequency cavities are preferred because [13][22][24]:

1. The highest average power rf sources are at 500 MHz and below.

2. For CW applications, which would become necessary for high-average power electron beams, cooling considerations for RT cavities favor lower frequencies. Although the heat losses are larger at lower frequencies, the larger cell surface area provides for more effective heat transfer.

3. The larger surface area per cell allows for more effective and simpler cooling of the cell walls.

4. Lower frequency cavities have the potential to produce higher quality electron beams for three reasons. First, for a given spatial length of each electron micropulse, it will span a

smaller $\Delta\phi$ phase of the rf accelerating fields which leads to more uniform acceleration properties. Second, the transverse dimensions (apertures) of the cavity are larger so the "transverse wake-field effects," or beam emittance induced in traveling through an aperture due to the image charges formed on the surface, is reduced. Third, the cells are physically longer since the length of a cell is approximately $\lambda_{rf}/2$. Therefore, for a given acceleration gradient, the beam will pass through fewer apertures to reach a given energy.

5. The volume of the cavity is proportional to λ_{rf}^3 so a reduced frequency leads to an increased cavity volume and higher stored energies. The electron beam traveling through the cavity creates higher order modes (HOM) by virtue of its charge. In higher energy density cavities, these HOM will disturb the cavity fields less and reduce the threshold of beam-breakup instabilities that can result.

6. Individual cavities can be more easily electromagnetically uncoupled which allows for better stabilization of the fields within.

The disadvantages of lower frequency operation are the increased size of the structure, and the fact that acceleration gradients must be lower. They are also more difficult to manufacture because of the increased size.

Figure 12 is a plot of equation 3.6 given values of $E_a = 10$ MV/m, $W = E \times L_a = 96$ MeV, $Q_{res} = 8\times10^9$, and $T = 4.2$ K. The minimum occurs at a frequency of 300 MHz. If Q_{res} or T decreases slightly, then this minimum will shift to higher frequencies. Therefore, a frequency of 400 MHz is a suitable design point for the SC accelerator. The wall losses for the SC structures will be approximately $P_L = 1.2$ kW. This value is insignificant to the overall power efficiency of the system. However, this value will determine the requirements for the liquid helium refrigeration support system.

The RT accelerator operating frequency is not as easy to determine. There are three criteria which determine the possible operating frequency range. First, the maximum field strength, $E_{\max}$, allowed within a cavity before sparking occurs is $E_{\max} \approx 1.5 E_{KP}/DM$ [23] where DM is an appropriate design margin and E_{kp} (MV/m) is the Kilpatrick sparking criteria field strength determined from the trancendental relation

$$f = 1.64\, E_{KP}^2\, e^{-8.5/E_{KP}}. \tag{3.9}$$

A design margin of four is generally used.

Second, a minimum field strength within the cavity is necessary to ensure adequate energy storage so that the energy removed in accelerating an electron pulse is a small fraction

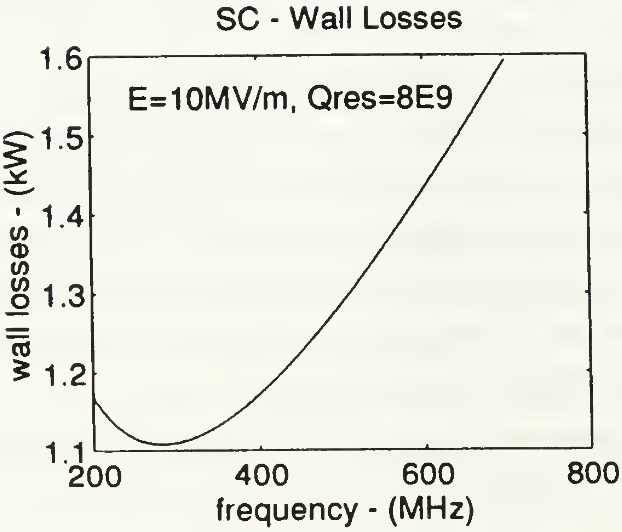

Figure 12 - SC accelerator wall losses

of the total cavity stored energy. This minimum field strength, $E_{\min}$ is given by [23]

$$E_{\min} = \frac{k_1}{k_2} \frac{2\pi f \ M \ I_{avg}}{(\Delta U / U)} \tag{3.10}$$

where $\Delta U / U$ is the fraction of energy removed from the cavity by an accelerating electron pulse and M represents the pulse repetition rate in integer numbers of rf cycles. A value of $M = 12$ means that an electron pulse is accelerated every 12^{th} rf cycle.

The final criteria needed to determine the operating frequency for RT structures is the maximum allowed wall losses, $P_{\max}$. Equation 3.7 establishes the relationship between E_a and f for a fixed P_L.

The relationship between these three criteria is shown in Figure 13(a) with values $k_1 = 3.5 \ M\Omega/m/MHz^{1/2}$, $k_2 = 8\times10^5 \ MHz^{1/2}$, $M = 12$, $I_{avg} = 500$ mA, $\Delta U/U = 0.02$, and $P_{\max} = 4$ MW. The $E_{a_{\min}}$ curve can be lowered only by changing M given the design constraints of our problem. Current accelerators operate with values of $12 < M < 20$. For a given value of M and $\Delta U / U$, the wall losses are less at lower frequencies because of the reduction in field strength. A value of $M = 12$ was chosen to be consistent with current

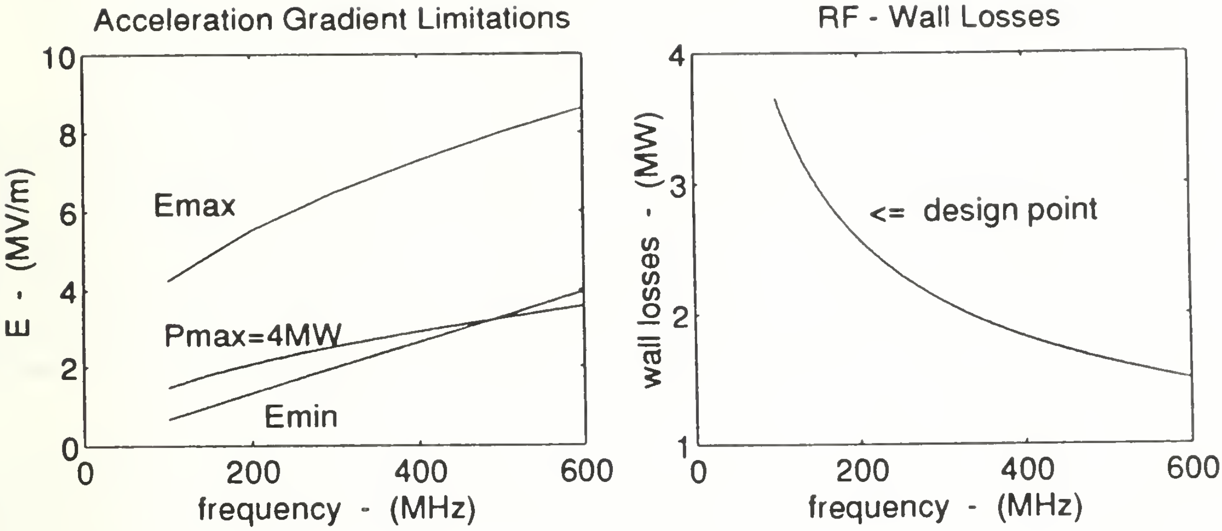

(a) (b)

Figure 13 - RT accelerator (a) field strength requirements, and (b) wall losses

technologies. As M is reduced, the peak currents are reduced as is the excitation of HOM within the accelerator cavities. However, less time is available to damp these modes out.

Within the design constraints of the FEL, a maximum rf frequency is desired to limit the wall losses in the RT structure. A maximum acceleration gradient is also desired in order to reduce the active length of the accelerator structure. However, this is limited by the resultant increased power losses. Therefore, an operating frequency of 200 MHz is chosen for the RT accelerator. From Figure 13(b), the wall losses are P_L = 2.9 MW with an E_a = 1.5 MV/m.

This analysis does not address the suitability of a structure with these parameters for use in an FEL. Extensive modeling and numerical simulations would be required to determine the beam quality and beam transport characteristics that could be achieved with such a structure. However, these parameters have been validated by a comparison to an actual 180 MHz cavity design [12].

It is prudent to note that the trend for future compact FEL accelerators is to include recirculation with energy recovery where a beam is bent around to pass through the accelerator two or more times to reach its final energy [2][13][25]. This allows accelerators to be more compact in that the active length of the accelerator is smaller by a factor approximately equal to the number of passes. The power estimates for these specific architectures will be nearly identical to the analysis presented here. However, the control system issues are more complex.

C. ELECTRON INJECTOR

The purpose of the electron injector is to produce high density pulses of electron current and inject them into the accelerator at the proper phase relation to the accelerating rf fields. The injector consists of two major components: the electron gun and the buncher. The buncher systems contain rf cavities similar to accelerator cavities. These cavities are designed to produce bunched electron pulses of low emittance. One of the most promising electron gun technologies for the production of high current, low emittance electron beams center on the dc photocathode [12][14].

Figure 14 shows the functional component interconnections of an injector driven by a dc photocathode electron gun. When illuminated by laser light, electrons are liberated at the photocathode through the photoelectric effect. A dc high-voltage rapidly accelerates the electrons away from the photocathode and directs them into the buncher. The dc voltage should be large to prevent the Coulombic space charge effects from inducing excessive initial emittance. However, since the electron velocity cannot exceed the speed of light, the voltage must be low enough to limit the electron velocity sufficiently below the speed of light when the electrons enter the buncher so it can effectively bunch the micropulses before they enter the accelerator [22]. A suitable value for the dc voltage is 500 kV. The electrons have been accelerated to a kinetic energy of about 500 keV (velocity, $v \approx 0.85c$) when they enter the buncher.

In describing the electron gun power requirements, it is more convenient to start at the high voltage dc electrodes and work back towards the drive laser. The high voltage has a practical limit due to dielectric breakdown effects and the emittance limiting effects previously mentioned. As buncher and high voltage power supply technology has improved, however, this voltage limit has also risen. Currently, and for the near future, these devices can be expected to operate at about 500 kV [2][14]. Therefore, for a 500 mA average electron current, 250 kW of high voltage dc electrical power must be supplied by the dc electric field to the electron current.

To generate the 500mA of average current, we use a photocathode which emits electrons via the photoelectric effect. It is assumed that our accelerator will be operating in the CW mode so that the peak currents in each micropulse is minimized. However, to minimize the beam emittance, the electron micropulses should have a spatial length corresponding to only a

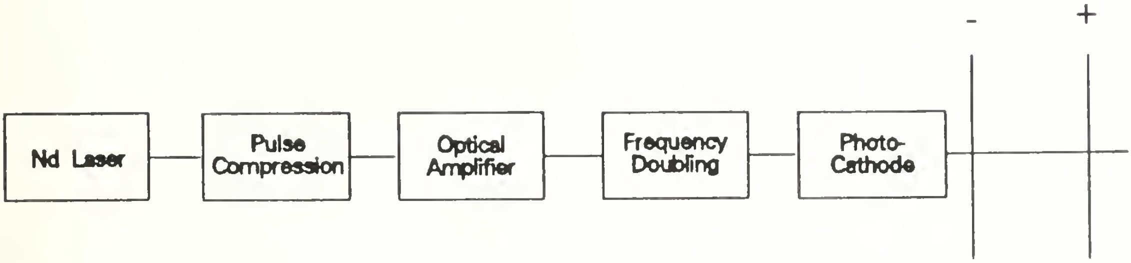

(a) typical dc photocathode electron gun

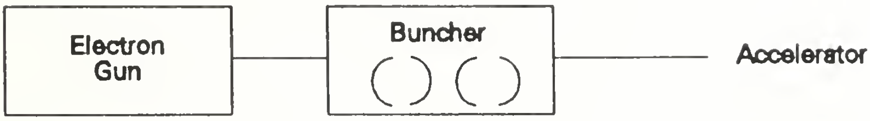

(b) electron injector

Figure 14 - typical electron injection system

few degrees of rf phase. Reference [22] defines a good injector as supplying a phase spread of $\Delta\phi \lesssim 10°$ and a very good injector as having a $\Delta\phi \lesssim 5°$. Low emittance electron beams are being produced with micropulse phase spreads of approximately $\Delta\phi = 5$–$6°$ [2][14][26]. For a CW 400 MHz system, a $\Delta\phi = 6°$ corresponds to a pulse length of 42 ps with an average micropulse current of 30 A per rf cycle. Therefore, we require an average electron charge of 1.25 nC per rf cycle or $1.25 \times M$ nC per micropulse. At a rf frequency of 200 MHz, we require an average electron charge of $2.5 \times M$ nC per micropulse. Electron pulses of 3-4 nC, peak currents of several hundred amps, and average currents of tens of mA have been effectively produced [26][2][14] with rapid advancements being made. The expectation of a 500 mA average current in the future is reasonable.

The photoelectric effect is described by

$$E_{ke} = h\nu + W_{pe} \tag{3.11}$$

where E_{ke} is the kinetic energy of the liberated electron, $h\nu$ is the energy of the absorbed photon, and W_{pe} is the work function of the photoemissive material. The values of the work functions for the different elements range from 3.14 eV (cesium) to about 6 eV [27]. This minimum photon energy required to generate a free electron means that photocathodes are insensitive to infrared radiation. The amount of charge liberated by a pulse of total energy E_p with photons of energy $h\nu$ is

$$q(\mathrm{n}C) = 10\ \frac{E_p(\mu\mathrm{J})\ QE(\%)}{h\nu(\mathrm{eV})} \tag{3.12}$$

where QE is the effective quantum efficiency which is the ratio of the number of liberated electrons to the number of incident photons. Table 4 lists the effective quantum efficiency for a number of photocathodes under development.

photocathode	QE (%)	$\lambda_{incident}$ (nm)	Comments
CsK_2Sb [26]	0.1	527	1-3 nC
Cu [UCLA]	.01	266	> 1 nC
Ag [29]	.03	248	
Cu+10%BaO [Aganofov]	.17	266	
LaB_6 [31][32]	.06	349	T = 1500 K
GaAs [14][2]	18	527	
CsTe [33][34][35]	13	263	long lifetime
CsTe [34][35]	19	251	

Table 4 - Photocathode quantum efficiencies

It is reasonable to expect that a photocathode will be developed suitable for a shipboard FEL with a quantum efficiency of QE = 20%. However, a QE = 5% would be a more conservative expectation, and would account for QE variations over the lifetime of the photocathode. From 3.12 we can show that the required laser input power to the photocathode to generate a required current is

$$P = \frac{h\nu(\text{eV})}{10\, QE(\%)}\, I(\text{mA}) \qquad (\text{W}) \tag{3.13}$$

For a frequency doubled Nd:YAG laser ($\lambda \approx 532$ nm) and a $QE \approx 5\%$, an average current of 500 mA would require an input power of 11.7 W incident on the photocathode.

The frequency doubler is a non-linear electrooptic crystal in which second harmonic generation occurs. If we align the crystal's crystallographic axes such that the index of refraction for both the fundamental and second harmonic frequencies are equal, the crystal is "phase-matched". Under the phase-matched condition, two photons of the fundamental essentially combine to form a new photon of twice the frequency, that is

$$\vec{k}_f + \vec{k}_f \rightarrow \vec{k}_{2f}$$

$$\hbar\omega + \hbar\omega = \hbar(2\omega) \tag{3.14}$$

The efficiency of frequency doubling, ranges from 20-65% depending on the input power level. Present photocathode electron guns operate with a frequency doubling efficiency, η_{fd}, of about 50% [26][14], but that can vary depending on the actual incident power intensity. For linac applications, the length of the electro-optic crystals are limited by group velocity mismatch which tends to increase the pulse length and limit the frequency doubling efficiency. Using type 1 phase-matching, however, efficiencies of more than 60% can be obtained [36]. Due to our high-power requirements, a frequency conversion efficiency of $\eta_{fd} = 55\%$ is assumed.

An optical amplifier is a pumped laser medium which amplifies the input signal through stimulated emission. An optical amplifier is described by the expression [37]

$$\ln(G_{sp}) + \frac{\Phi(0)}{\Phi_s}[G_{sp}-1] = \beta_o d \tag{3.15}$$

where β_o is the unsaturated gain coefficient, d is the single pass length of the amplifier medium, G_{sp} is the overall single pass gain, Φ_s is the saturation photon flux density, and $\Phi(0)$ is the input photon flux density. Φ_s is a function of only the amplifier medium while β_o is a function of the amplifier medium and is directly proportional to the population inversion per unit volume. Therefore, β_o will determine the power requirements for the amplifier.

To maximize the power efficiency of the amplifier, the amplifying medium must be efficiently pumped and multiple passes must be made by the light wave through the amplifying medium. To efficiently pump the medium, laser diode pumping provides the most efficient method because the pump energy is concentrated at the pump bands of the Nd lasing medium. The width of the diode pump spectrums are on the order of 5 nm FWHM [38]. Furthermore, diode lasers, driven by a low dc voltage, can achieve a quantum efficiency of near unity [39][40]. One particular diode-pumped optical amplifier design utilizing a confocal, parabolic mirror cavity with an internal Brewster plate to increase the path length of the beam within the crystal, has achieved small signal gains of 38 dB with a pump to optical power efficiency of 40% for the Nd:YLF medium and 25% in the Nd:YAG medium operating in the CW mode [41]. Amplified spontaneous emissions are only about 1% of the total output power. The Nd:YAG amplifier, however, was able to support much more pump power than the YLF amplifier which fractured at lower pump powers. For the estimation of amplifier power requirements, it is assumed that an optical amplifier for my FEL photoinjector has a pump power amplification efficiency, η_{amp}, of 25%.

Nd:YLF and Nd:YAG mode-locked CW lasers are commonly used as photoinjector drive lasers because they are relatively rugged, produce short pulses (about 75 ps for YAG [39] and 50 ps for YLF [42]), have large optical gain per unit distance, and can be easily amplified. The large optical gain means they have a low threshold power required for CW operation. With laser diode pumping, we can achieve much higher pumping efficiencies. The resulting inefficiencies are predominantly due to incoupling losses, the fraction of energy absorbed by the lasing medium, and the spontaneous emission losses. Optical-to-optical efficiencies of the diode-pumped laser have been demonstrated at 25% for Nd lasers in CW mode [43]. Diode lasers delivering 60 W for a 200 μsec duration are commercially available. Advances in the development of higher-powered diode lasers and improvements in the coupling optics are expected to lead to pulse durations below 10 nsec in the near future [43]. This is sufficient to support the 42 ps pulse lengths needed to support this FEL.

Current Nd drive lasers used in photocathode electron guns have self phase modulation (SPM) pulse compression systems with an incoupling loss of 25% [42]. These guns drive accelerators operating at rf frequencies of several GHz where narrow electron pulses are required. The pulse compression systems do not require input biasing or pumping power but do limit the peak output power from the laser to about 2 W. Pulse compression systems, however, should not be required for the low accelerator frequencies under consideration for a high-power FEL. If we assume a laser output power of 2 W at a wall plug efficiency of 25%, only a few watts of power are needed. Therefore, the drive laser power and pulse compression losses can be neglected from the prime power analysis.

The power requirements of the electron gun now can be summarized in terms of Figure 15. The total required low voltage dc power, P_{Ldc}, is given by

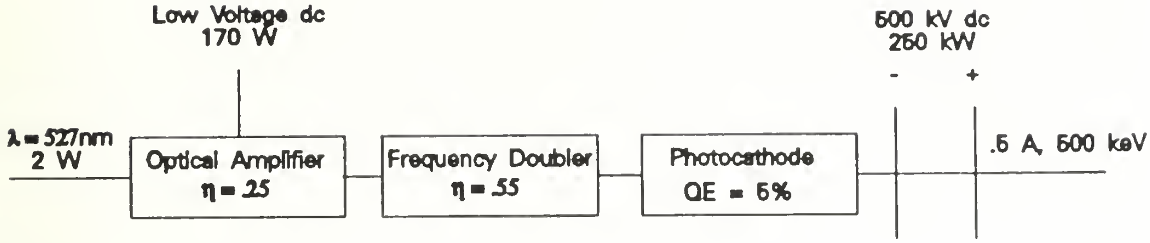

Figure 15 - Power flow in the dc photocathode

$$P_{Ldc} = \frac{1}{\eta_{amp}} \frac{1}{\eta_{fd}} \frac{h\nu(\mathrm{eV})}{10\ QE\,(\%)}\ I_{avg}(\mathrm{mA}) \qquad (\mathrm{W}) \tag{3.16}$$

and the total high voltage dc required, P_{Hdc}, is the average current times the voltage applied. For a 500 mA average current and 500 kV acceleration, we will require P_{Ldc} = 170 W and P_{Hdc} = 250 kW.

The buncher cavities are RT cavities whose geometry and fields are optimized to provide bunching of the electrons into micropulses with low emittance and energy spread. SC cavities and their associated geometries are not efficient for this purpose so RT cavities are used exclusively. The electrons liberated from the photocathode are bunched longitudinally and focused to a waist as they are injected into the accelerator. Solenoidal magnetic fields are also used to assist the bunching process.

For the defined architecture and parameters, the buncher cavities must provide 3 MeV acceleration to the electrons during this bunching process. Since the electrons are entering the buncher at a velocity of $v \approx 0.85c$, the fields must be rather strong to bunch the electrons. To determine the wall losses in the buncher, P_{Linj}, the same model used for estimating the accelerator wall losses is employed. To achieve 3 MeV acceleration, three cavity cells at a frequency of 200 MHz and E_a = 1.33 MV/m is assumed. To account for added losses due to the required geometry changes, the shunt resistance constant is assumed to be k_1 = 1.9 (MΩ/m/MHz$^{1/2}$). Therefore, we can estimate $P_{Linj} \approx$ 150 kW. At a frequency of 400 MHz, only 100 kW of power would be dissipated.

Although electromagnets are often used to produce the solenoidal fields, large permanent magnets with small tuning electromagnets would be more appropriate for high-current applications. Therefore, they will not add significantly to the power requirements.

D. RF SYSTEMS

Electron accelerators have historically operated at rf frequencies of more than 1 GHz, low average power, and high peak powers in a pulse power electron beam format. Klystrons have been the only rf sources suitable for these operating conditions. For rf frequencies of 200-500 MHz, however, additional rf sources may be practical.

Table 5 is a listing of several of the most powerful CW klystrons currently on the market.

	TH2089	YK1350	YK1303	K3513	Units
Reference	[44]	[44]	[44]	[45]	
frequency	352	352	508	352	MHz
input voltage	87	90	90	100	kV
input current	17.1	16.8	18.2	20	A
Power	1	1	1	1.3	MW
efficiency	68	66	61	65	%
length	4.75	3.75	3.75	4.2	m

Table 5 - Commercially available super-power CW klystrons

Klystrons have evolved over several decades so revolutionary advances in their power capabilities within the next 20 years are not anticipated. Some of these tubes are designed to operate in a vertical orientation while others are designed to operate in a horizontal orientation. High-power klystrons are available in either configuration. The output power and power conversion efficiency of a klystron for a shipboard FEL can be expected to have an output power of about 1.5 MW at an efficiency of 65%.

Some alternative rf sources for accelerator applications are listed in Table 6. The high-power entries in this table are projections and have yet to be developed. However, these alternate technologies promise rf sources that operate at lower voltages, higher efficiency, and

	MBK	MBK*	klystrode	klystrode*	IOT	Units
Reference	[46]	[46]	[47]	[48]	[49]	
frequency	425	500	267	476	476	MHz
input voltage	17	39	65	25	66	kV
input current	11	41	5.5	70	9.3	A
Power	0.1	1	0.25	1.3	0.4	MW
efficiency	55	64	70	75	> 65	%
length	1.35	2.5	NA	NA	2.1	m
	400	800	NA	NA	500	kg

Table 6 - Alternative CW rf power sources (* - denotes projection and is not commercially available)

have a reduced component weight and volume. It is expected that the multiple beam klystron (MBK) efficiency can be increased to >80% with further development [24]. The klystrode and inductive output tube (IOT) are essentially the same device with klystrode being Varian Associates trademark for this device. It has the disadvantage of a smaller gain. Therefore, a larger rf drive is required for the device (several kW for a megawatt device). This will add to the complexity of the overall rf system.

E. SUPPORT SYSTEMS

A wide variety of support systems will be required for a shipboard FEL. Feedback control systems will be required to maintain rf power source phase and amplitude stability. The 2.5 MW of heat energy dissipated in the beam dump and the 3 MW of heat energy dissipated in the RT structure as wall losses will need an appropriate cooling system. System monitoring and fire-control interconnections will also place a load on the ship's electrical system. These systems, however, can easily be adapted to existing shipboard systems. Current steam propulsion plants dump heat energy well in excess of 50 MW at a cost of tens of kW of seawater pump power. Therefore, a reasonable estimate is that these systems will add an additional 100 kW to the ship's electrical load.

There are three support systems, however, that need to be addressed separately. First, a SC structure will require a liquid helium refrigeration system. The power requirements for this system can be estimated by [17]

$$P_R = P_L \frac{T_a - T_{He}}{T_{He}} \frac{1}{\eta_R} \tag{3.17}$$

where P_R is ship's service AC power consumed by the refrigeration system, T_a is the ambient (room) temperature ($T_a \approx 300K$), T_{He} is the liquid helium boiling point temperature ($T_{He} \approx 4.2K$), and η_R is the refrigeration efficiency. The second term in 3.17 represents the Carnot thermodynamic efficiency of the system and the third term is the refrigeration system (compressor, etc.) efficiency. Typical values of η_R are approximately 25-35 percent [14][16]. For a 30% efficient refrigeration system removing a P_L = 1.2 kW, our shipboard FEL will require $P_R \approx (235 \times P_L) \approx$ 250 kW of refrigeration power if the laser were to operate continuously. This is not only a significant amount of power but the size of the refrigeration plant would be large [2][14].

The refrigeration plant for this shipboard FEL, however, can be considerably smaller since it will not operate continuously. The rate of liquid helium boiled off during FEL operation is

$$\dot{V} = \frac{A}{\rho\, q_v} P_L \tag{3.18}$$

where $\dot{V}$ is the rate of helium boiled of during laser operation (gal/sec), A is the atomic weight of helium (4 g/mole), ρ is the density of helium at T_{He} (7.62 $\mathrm{lb/ft^3}$), and q_v is the latent heat of vaporization of helium (84 J/mole). The operational requirements specify that the FEL must operate for 150 seconds over a 20 minute interval. Conservatively assuming that the laser operates continuously for 150 seconds with a wall loss of P_L = 1.2 kW, 18.5 gal of liquid helium is boiled off. This is a relatively small amount of required stored liquid helium. Therefore, the refrigeration system can be designed to recompress and refrigerate this boil-off over a longer period.

The refrigeration system sizing criteria, therefore, is based on two factors. First, the refrigeration system must be able to remove the latent heat of vaporization from the helium boiled off during laser operation within a specified time period. Arbitrarily choosing this time period as 2 hours, then the refrigeration power required is

P_R = 250 kW (100 sec/2 hrs) = 3.5 kW. Most importantly, the refrigeration system size and weight has been reduced significantly. A reserve storage capacity of liquid helium can reduce this requirement even further. The second factor is the time required to reduce the temperature of the accelerator from room temperature to operating temperature following an import maintenance period. To perform this cooldown within 48 hours would require a refrigeration system that would be excessively large for the shipboard environment [14]. A shore facility could perform this cooldown prior to a warship getting underway and eliminate the need for this sizing criteria.

The second support system that needs to be addressed is the network of electron beam bending magnets which control the beam trajectory. Large permanent magnets would also be appropriate for this purpose. Although they are much more expensive, they require no external electrical power source. If electromagnets were used and a magnet failed, the beam would impact the wall of the beam tube creating a large radiation hazard for adjacent personnel and causing a shutdown of the FEL.

The final support system deals with the optical resonator. The resonator will have megawatts of power circulating between the mirrors. Special mirror configurations have been designed for high-power applications [2] to reduce the power intensity on the mirrors and the onset of damage. The optics will need, however, an active stabilization system to maintain alignment during ship vibrations, flexing, and torsional movements. Furthermore, neglecting outcoupling of the laser light, the mirrors will also absorb some energy and need a cooling system. Mirrors have been developed with a reflectance of 99.975% at λ = .87 μm [50]. In general, mirror reflectivity improves as the optical wavelength moves into the infrared. Assuming a reflectance of 99.9% with a resonator stored power of 5 MW, 5 kW of energy is absorbed in the mirrors. Suitable stabilization and cooling systems have already been developed [24][51]. The power requirements can be included with the overall support system power allocation, P_{ss}, of 100 kW.

F. SUMMARY OF POWER REQUIREMENTS

The power requirements for the FEL architecture of Figure 10 under the design constraints of a naval application are summarized in Table 7. Since about 95% of the electron beam power is recovered in this architecture, the listed power requirements are nearly independent of the output power level. For example, the accelerator wall losses are solely a function of the stored cavity field strength. Therefore, the wall-plug efficiency of the FEL scales as the output power. The rf source efficiency is based on commercially available

parameter	SC value	RT value	units
f	400	200	MHz
W_b	100	100	MeV
I_{avg}	500	500	mA
E_a	10	1.5	MV/m
Z	311	990	Ω/m
Q_{res}	5×10^9		
Q_o	3×10^9	5×10^4	
P_{Ldc}	350	350	W
P_{Hdc} @ 500 kV	250	250	kW
P_{inj}	2	2	MW
P_{Linj}	150	150	kW
P_{beam}	50	50	MW
η_o	2	2	%
P_{out}	1	1	MW
P_{ret}	49	49	MW
η_{rec}	95	95	%
P_{dump}	2.45	2.45	MW
P_{rec} @ $\eta_{rec} = .95$	46.6	46.6	MW
P_L	.0012	2.9	MW
P_R @ $\eta_R = .3$	275		kW
P_{RF} @ $\eta_{RF} = .65$	6.6	9.2	MW
P_{ss}	100	100	kW
wall-plug efficiency	17.4	10.4	%

Table 7 - Summary of the power requirements for a shipboard FEL

klystrons. Alternative rf sources promise an increased efficiency but require further development before they can produce high-average power. If extrapolations are made to higher power for these devices, then the FEL total power requirements can be reduced by about 10%.

For the RT accelerator, it was necessary to define the pulse repetition interval represented by the parameter M to determine the accelerator operating frequency and wall losses. From equation 3.10 and Figure 13 it can be seen that reducing the value of M can reduce the RT cavity wall losses. However, the optical resonator must have dimensions set so that when an electron pulse passes through the undulator, it overlaps with an optical pulse and can transfer energy to the optical field. Therefore, the mirrors must be separated by a distance $L = \mathrm{n}Mc/2f$, where n is an integer and equals the number of optical pulses stored within the resonator cavity. For the values in Table 7 and assuming $M = 12$, $L = 9\mathrm{n}$ meters for the RT accelerator parameters. If the resonator cavity was 18 meters long, then there would be two optical pulses circulating within the resonator.

For the SC accelerator based FEL, M is not an important parameter in determining power losses or the rf frequency because of the high cavity Q and large accelerating field strengths. However, the pulse repetition rate will affect the length of the resonator in the same way as for the RT accelerator based FEL. For the SC parameters defined in Table 7, and assuming $M = 12$, the resonator length is $L = 4.5\mathrm{n}$ meters.

IV. PRIME POWER DISTRIBUTION

In the previous chapter, the power requirements for a megawatt FEL laser weapon for shipboard applications were outlined. The two components that burden the prime power distribution system are the dc photocathode high voltage and the rf sources for the electron rf accelerator. It was determined that the dc photocathode would require 250 kW at 500 kV dc while the rf sources would require 6-10 MW at 80-100 kV dc. This amount of power cannot be delivered through the conventional ship's service power distribution system. In this chapter, the characteristics of a shipboard prime power distribution system capable of delivering power to these FEL components are explored.

The prime power supply requirements are summarized in Table 8. These requirements are established to be consistent with the FEL power requirements of Chapter III.

	rf sources	dc photocathode
voltage	100 kV	500 kV
power	10 MW	250 kW
type	dc	dc
duration	15 sec	15 sec

Table 8 - Prime power requirements to support a high-power FEL

The value of 100 kV for the rf source input voltage was chosen to support the high-power klystron operation. This is a limiting value and would likely be about 40 kV when alternate rf sources are developed.

A. POWER GENERATION AND DISTRIBUTION

The FEL system will require a dedicated distribution bus. Therefore, this bus is not limited to the normal ship's service distribution system operating parameters of 450 V, 3 phase, and 60 Hz. Several studies have been performed to outline the prime power system for high-power, electrically-powered weapons with power requirements similar to FELs [52][53][54][55][56]. The power generation and distribution aspects of these studies are equally pertinent to this discussion and are summarized in this section for continuity purposes.

Follow-on sections will address components specific to the FEL systems.

The prime power distribution system is illustrated in Figure 16. Power generation and distribution component weights and volume are summarized in Table 9. Power is diverted from a propulsion gas turbine engine to an auxiliary generator to power the FEL distribution bus. Modifications to the pinion that connects the turbine to the main reduction gears have been designed so that the turbine power is automatically diverted to the auxiliary generator without operator action when load is drawn by the FEL loads [52][53]. Simulation studies have shown that this diversion of power will only cause a momentary reduction of ship speed of a few percent when operating at flank speed over the duration of the laser shot [53]. The IED generator pictured in Figure 16 represents the electrical generator which would power an electric drive ship. This element would be deleted for a ship powered with mechanical drive where the propeller shaft is directly coupled to the reduction gears.

The FEL distribution bus would operate at about 5 kV, 3 phase, 800 Hz. As bus frequency is increased, the size and weight of generator and transformer components are reduced. However, their efficiency is also reduced. A frequency of 800 Hz was determined to be the best compromise between these two competing factors [52][55]. The 5 kV bus voltage was chosen due to conductor sizing limitations. A low bus voltage causes the transmitted current to be high resulting in the need for large cable conductors. Similarly, a large voltage results in increased cable size due to insulation requirements.

B. 20 MVA TRANSFORMER

Computer algorithms have been developed for the prediction of transformer weights for a pulsed, high-power electrical load. Over a power range of 10-50 MW, the weight of an adiabatic (no forced cooling) transformer is given by the expression [57]

$$\text{Weight} = 0.0505\ (t/120)^{0.337(V_o/100)^{-0.0413}} * [0.693 + 0.307\ (P/25)^{-0.79}]$$

$$* [0.931 + 0.069\ (V_o/100)^{1.3}] * [0.242 + 0.758\ f^{-0.926}] \quad (\text{lbs/kW}). \quad (4.1)$$

For a 1-5 MW transformer, the weight is given by

$$\text{Weight} = 0.1275\ (t/120)^{0.281} * [0.693 + 0.307\ (P/25)^{-0.79}]$$

$$* [0.931 + 0.069\ (V_o/100)^{1.3}] * [0.242 + 0.758\ f^{-0.926}] \quad (\text{lbs/kW}) \quad (4.2)$$

where t is the total run time (sec), P is the power level (MW), V_o is the dc load voltage (kV) assuming rectification without phase-control at the output of the transformer, and f is the bus

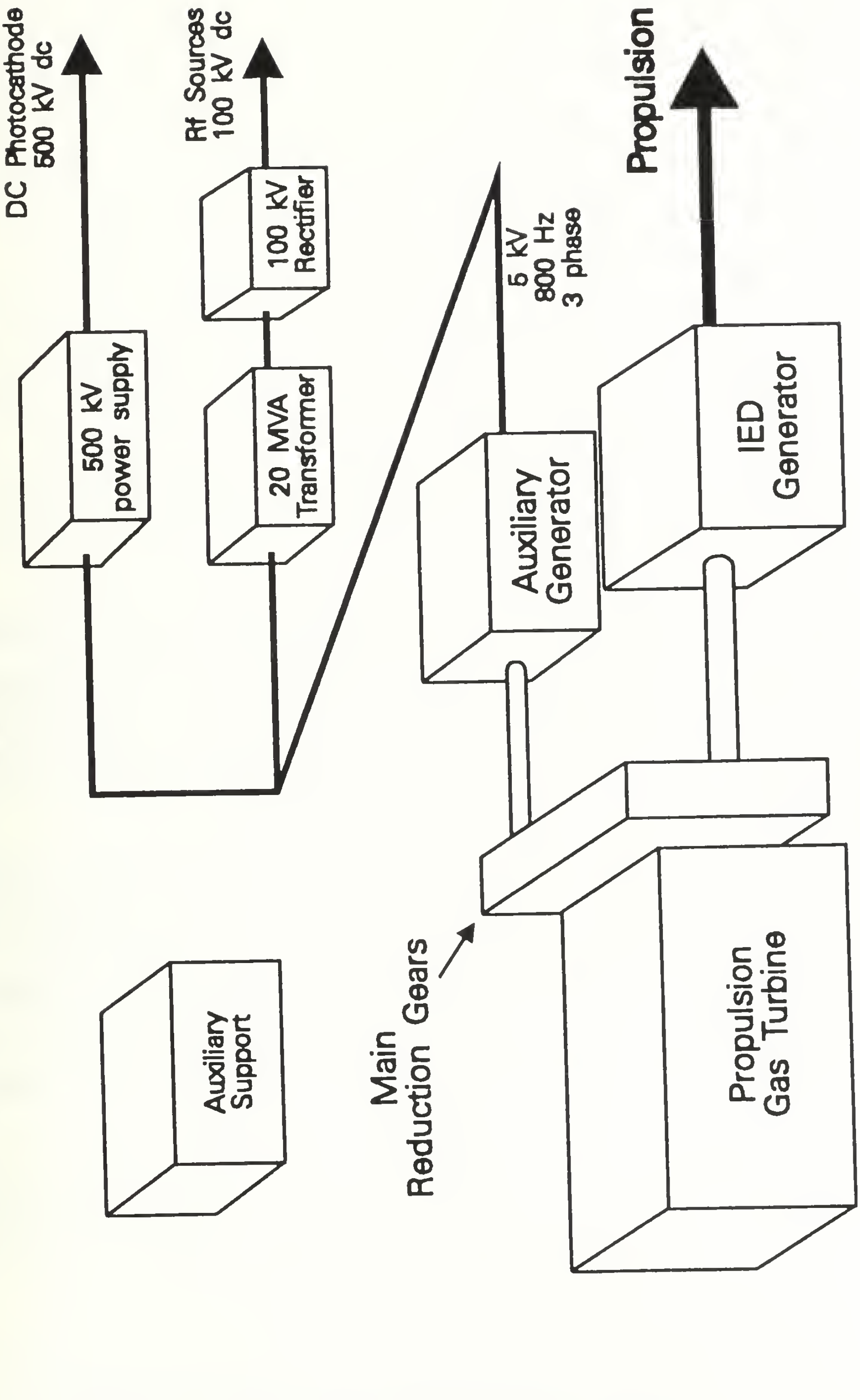

Figure 16 - Prime power distribution system. After Ref. [52]

component	weight (kg)	volume (m^3)
gas turbine	20,400*	46*
Main reduction gears	6800*	3.8*
auxiliary generator	8000	4.3
transmission cable	4500	1.0
auxiliary support	3300	NA

Table 9 - Summary of power generation and distribution component weights and volume. * - part of propulsion system and does not add to FEL system totals; NA - not available

frequency (kHz). These equations assume an input voltage of 1-5 kV and have been validated for output voltages of 20-200 kV, run times of 1-120 seconds, off times of 2-300 seconds, and frequencies up to 2 kHz. The studies which produced these relations also showed that adiabatic transformers provide for the lowest size and weight transformer characteristics for pulsed-power applications.

In order to conform with Navy standards, all components must be derated. The derating factors for both current and voltage are 0.7. The transformer which will supply the 10 MW bus for the rf sources was derated by $(0.7)^2$. Therefore, it was rated at 20 MW. From equation 4.1, the required 100 kV, 20 MW transformer would weigh 620 lbs (280 kg). The weight of a 100 kV, 2 MW transformer would be 157 lbs (71 kg). Therefore, there is a definite weight advantage to using a single transformer to supply a single 100 kV bus instead of using a few smaller ones.

A volume determination can be made from the method described in Ref. [55]. Figure 17 in Ref. [55] gives the volume of a transformer as a function of frequency and power level. From this curve, the 20 MW transformer would occupy approximately 5 m^3.

C. 100 KV RECTIFIER

The rectifiers were assumed to be composed of silicon-controlled rectifiers (SCRs) instead of diodes. This is because the accelerator rf sources and dc photocathode voltages need to be controlled to tight tolerances. Use of a phase-controlled rectifier allows for a control system to regulate the output voltage. The weight of the 100 kV rectifier was estimated to be 1500 kg while the volume was estimated to be 8 m^3. The analysis used to determine these values is presented in the Appendix.

D. 500 KV POWER SUPPLY

The 500 kV power supply must provide an average current of 500 mA. A voltage multiplication circuit would provide better performance [12] and be smaller and lighter than an equivalent transformer and rectifier combination. The weight and volume of a 500 kV voltage multiplier was estimated to be 4100 kg and 3 m^3, respectively. The analysis used to determine these values is presented in the Appendix.

E. ENERGY STORAGE

An important consideration for any weapons system is how it operates under casualty conditions. A dedicated energy storage element could provide a limited capability for FEL operation should the normal power distribution be interrupted. Several methods of energy storage were considered; storage batteries, superconducting magnetic energy storage, flywheels, and capacitor banks. Only capacitor banks are adequate to deliver megawatts of power within a fraction of a second and yet be compatible with the shipboard environment. The weight and volume of high-energy storage capacitors is proportional to the storage capacity. Modern capacitors can store 3 KJ/kg [53] and it is anticipated that 4 KJ/kg is achievable with some development [54][58]. These capacitors would occupy a volume of 5 MJ/m^3 [53][58].

The run time of 15 seconds for the FEL is based on the time available to engage a target and not on the laser dwell time required to destroy the target. Therefore, it may not be necessary to store enough energy for a full 15 second engagement. 20 MJ of stored energy would provide for a limited 2 second engagement. This amount of stored energy would require a capacitor bank that weighs 5000 kg and occupies 4 m^3. This capacitor bank would also require a power electronics package on the order of the 10 MW rectifier system in size and weight. The detailed estimates of this package were not made.

F. SUMMARY OF FEL PRIME POWER DISTRIBUTION

The weight and volume estimates for the prime power distribution system is summarized in Table 10. Those components which are normally part of the propulsion train are not included. The transformer and rectifier values were determined for a 100 kV FEL bus voltage.

component	weight (kg)	volume (m^3)
power generation	15800	5.3*
transformer	280	5
rectifier	1500	8
500 kV power supply	4100	3
totals	21680	21.3

Table 10 - Prime power weight and volume estimates. * - does not include auxiliary support equipment

These weight and volume estimates can be reduced appropriately as alternate rf sources become available.

Energy storage is not included in this summary. However, its inclusion would result in an increase of more than 5000 kg and 5 m^3 to the totals. This would be a significant increase in overall system size and weight.

V. HIGH-POWER FEL OPERATION

In the previous chapters, the design constraints and prime power considerations for a shipboard high-power FEL have been outlined. Various electron beam parameters have been defined so that an FEL could provide a 1 MW optical output. In this chapter, the conversion of electron beam energy to optical energy is explored. The undulator parameters considered in this chapter are not meant to specify a required design but to demonstrate that the defined electron beam parameters can, in fact, produce the desired output. Both the undulator and optical resonator parameters are also constrained by the overall system goals of minimum size and weight.

The electron beam parameters that must be considered to adequately characterize the FEL operation are summarized in Table 11.

parameter	value	units
Beam energy, W_b	100	MeV
Peak Current, I_{peak}	360	A
M	12	-
Micropulse length, L_e (400 MHz)	42	psec
Micropulse length, L_e (200 MHz)	84	psec
Beam radius, r_b	330	μm
Energy spread, $\Delta\gamma/\gamma$	0.002	-
ε (rms)	0.1	mm-mrad

Table 11 - Electron beam parameters

The electron beam radius, r_b, the electron beam energy spread, $\Delta\gamma/\gamma$, and the electron beam emittance, ε, are estimates made from existing accelerator electron beams. A high quality electron beam from a 1.5 GHz accelerator with a peak current of 200 A has the values $r_b = 164$ μm, $\Delta\gamma/\gamma = 0.1\%$, and an $\varepsilon = 0.1$ mm-mrad [2]. The electron beam radius and emittance scale approximately as the current [12]. It has already been established that emittance is reduced in lower rf frequency accelerators. Furthermore, electron energy spread $\Delta\gamma$ is conserved as an electron beam is accelerated [22]. Therefore, values of $r_b = 330$μm,

$\Delta\gamma/\gamma = 0.002$, and $\varepsilon = 0.1$ mm-mrad are reasonable assumptions.

A. FEL OPERATION - 3 μm WAVELENGTH

The operating wavelength of an FEL is determined by the resonance condition, equation 2.6, where $K = e\bar{B}_o\lambda_o/2\pi mc^2$. For operation at $\lambda = 3$ μm, a range of FEL undulator parameters are summarized in Table 12. These parameters were defined in Chapter II, sections A and D.

λ_o (cm)	K	ξ	$K_L(\xi)$	B_o (peak) (kG)
1	4.7	.48	3.3	71
3	2.6	.43	1.9	13
5	1.9	.39	1.5	5.7
10	1.1	.28	.96	1.7

Table 12 - Undulator parameters for FEL operation at $\lambda = 3$ μm

The undulator field strength is limited by technology. The maximum peak undulator field strength that can be produced is given by the expression [59]

$$B_o = 33.3\, e^{-\frac{g}{\lambda_o}\left(5.47 - 1.8\frac{g}{\lambda_o}\right)} \quad (kG) \tag{5.1}$$

where g is the gap between the pole pieces of the undulator magnets. The strongest field strength that has been manufactured in an undulator was $B_o = 18$ kG with a $g/\lambda_o = 0.11$ [60]. The minimum gap distance is determined by the transverse dimension of the optical mode. Under these limitations the minimum undulator wavelength that can be considered for this high power FEL is $\lambda_o \approx 3$ cm with a $g \approx 5.4$ mm.

The electron micropulse passing through the undulator is several hundred slippage distances long. Hence, the optical pulse will be approximately the same length as the micropulse and the duty cycle between pulses will also be equal. For the parameters of Table 11, the duty cycle, d, will be about 1/720. The optical pulse amplitude and phase characteristics will be periodic along the length of the pulse with a period of about one slippage distance. Therefore, simulation of the FEL electron-optical interaction over one slippage distance is sufficient to model the entire pulse.

The relationship between average power output of the optical resonator and the complex field strength is given by

$$P_{avg} = \pi w_o^2 d \, \frac{c}{4\pi} \left[\frac{\gamma^2 mc^2}{4\pi e N L K_L(\xi)} \right]^2 (1-e^{-1/Q}) \; |a|^2 \quad (\mathrm{kW}) \tag{5.2}$$

where Q is the quality factor of the optical resonator. Over the length of the undulator, however, the complex field strength and optical mode cross-sectional area are not constant due to diffraction effects. This variation is a direct function of the Rayleigh length, z_o. For a high-power FEL, we want z_o and w_o to be as small as possible to minimize the power density on the resonator optics. However, if $w_o < r_b$, then the gain of the FEL is reduced since not all of the electrons can interact with the optical mode. As explained in Chapter III, section E, this is accounted for by setting $j = j\,F$, where $F = (r_b/w_o)^2$, when simulating the wave equation. The value w_o, however, is dependent on the Rayleigh length of the optical resonator. Assuming Gaussian beam propagation, the value $z_o \approx L/\sqrt{12}$ minimizes the volume for the optical mode over the length of the undulator and provides for maximum gain when $w_o \gtrsim r_b$ [5]. With $z_o = L/\sqrt{12}$, we can use equation 5.2 and neglect the variation in $|a|$.

The optical parameters for several undulators are listed in Table 13. The Rayleigh length of the resonator is assumed to be $z_o = L/\sqrt{12}$.

λ_o (cm)	N	L (m)	w_o (mm)	j
3	15	.45	.35	6.3
	25	.75	.46	17.6
4	15	.6	.41	6.3
	25	1	.53	17.4
5	15	.75	.46	6.2
	25	1.25	.59	17.1

Table 13 - Optical parameters for FEL operation at $\lambda = 3\ \mu m$

Several simulations were performed to determine the relationship between j, $|a|$, and Q. The results of these simulations for values of $j = 4$, 7, and 13 are shown as curves in Figure 17. Overlayed with these curves is the $|a|$ vs. Q relation determined by equation 5.2 for a 1 MW optical output and an undulator with $\lambda_o = 3$ cm, $N = 16$, and $j = 7$.

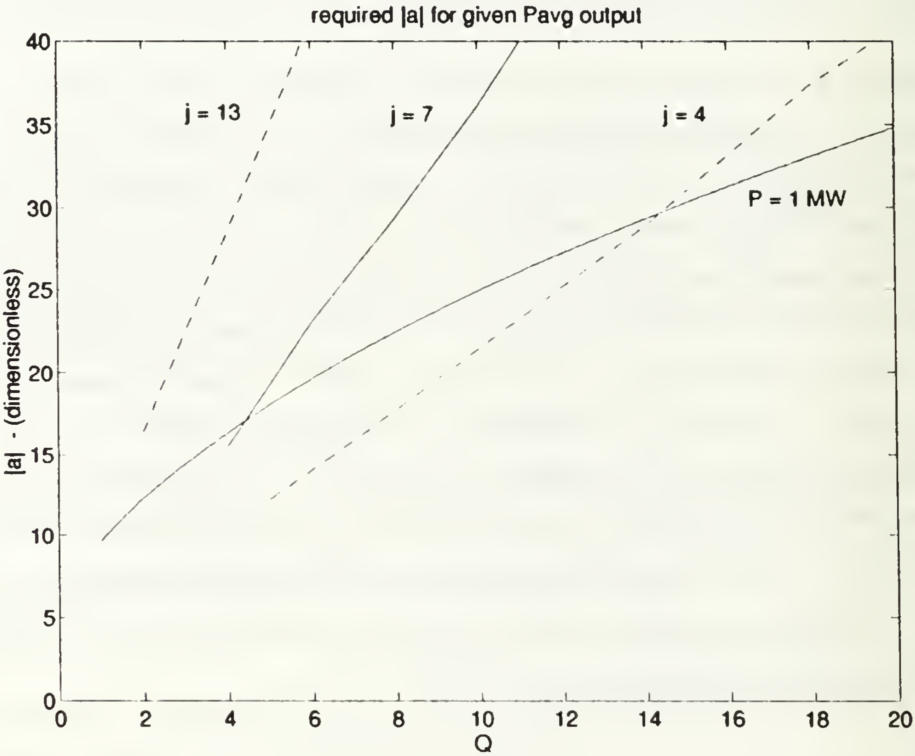

Figure 17 - $|a|$ vs. Q dependence for several values of j. The curve marked "P = 1 MW" is the $|a|$ vs. Q relationship for an undulator with $j = 7$, $\lambda_o = 3$cm, and $N = 16$. The intersection of the two solid curves is the required operating point

The optical mode within the resonator must have an $|a| \approx 17$ and the resonator must have an outcoupling of 20% ($Q \approx 4.5$). From Figure 17, it is obvious that more than 1 MW can be extracted from the electron beam by increasing the resonator Q. However, this would result in an undulator extraction efficiency of more than 2%.

The average power within the resonator cavity is 5 MW and is contained within an optical mode size of $w_o = 0.364$ mm. Assuming a Gaussian profile, essentially all of the power ($\lesssim$ 100 W) is contained within a cross-section of $8w_o = 2.7$ mm at the ends of the undulator where the spot size is largest. Allowing for alignment tolerances, the undulator gap distance g = 5.4 mm is adequate.

B. ANALYSIS OF FEL OPERATION

The FEL saturates at an average power of 1 MW for j = 7 and $Q \approx 4.5$. The steady state characteristics of the FEL interaction are shown in Figures 17, 18, and 19. Figure 18 is the gain and phase curve, as defined in section H of Chapter II, for this FEL near saturation. The undulator's sensitivity to electron beam quality, as explained in section G of Chapter II, is proportional to the number of periods. Therefore, the gain curve is virtually insensitive to beam quality since the undulator only has 16 periods. Figure 19 is the phase space evolution of an electron pulse at saturation. Approximately 60% of the electrons are trapped in closed orbits. The trapped electrons leave the undulator with phase velocities concentrated about $\nu \approx -5$ while the non-trapped electrons exit with phase velocities spread about $\nu \approx 5$.

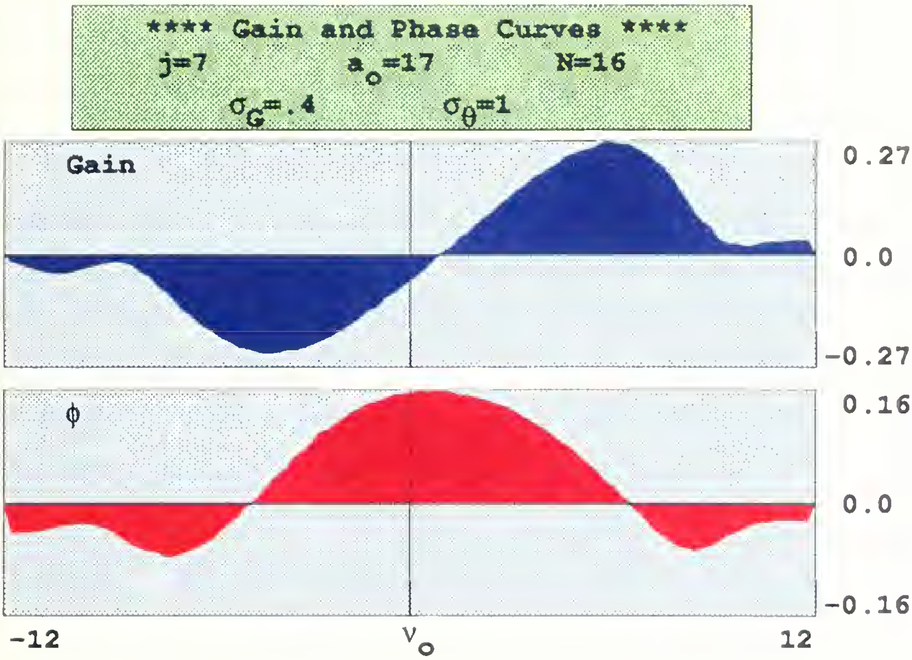

Figure 18 - Gain spectrum at saturation for operation at λ = 3 μm

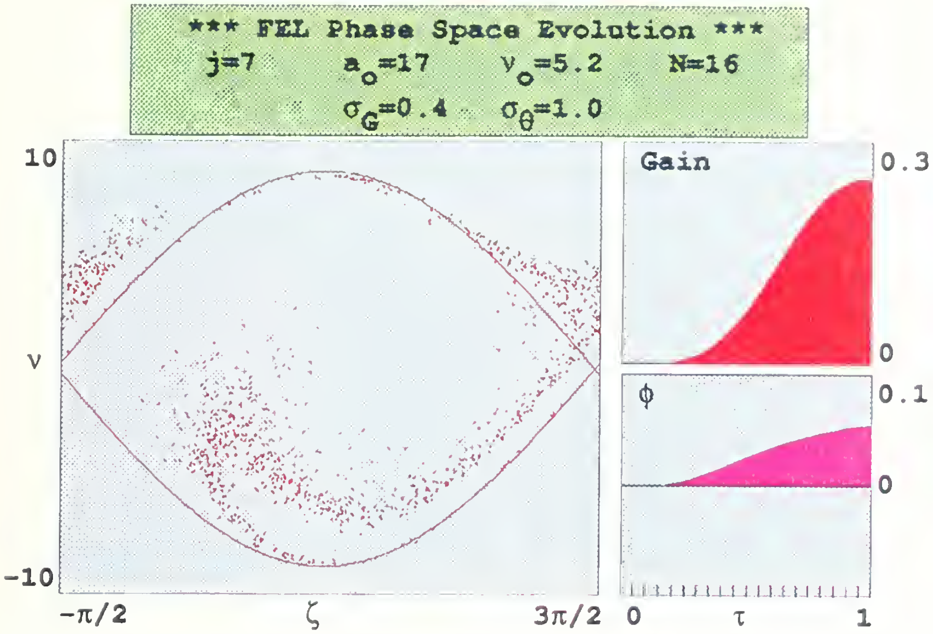

Figure 19 - Phase space evolution at saturation for operation at $\lambda = 3\ \mu m$

The startup characteristics of the FEL are illustrated in Figure 20. The evolution of the optical mode over n = 150 micropulses beginning from spontaneous emission is shown. The left window shows the complex field strength over one slippage distance, the center window shows the power spectrum, and the right window shows the electron distribution. The electron distribution of this simulation agrees with the phase space distribution of Figure 19 in that the electrons are concentrated in two distinct phase velocity groups. The power spectrum has a single mode and so there is no modulation of the complex field strength envelope. The steady-state complex field strength is $|a| = \sqrt{P(n)} \approx 17$. The optical field reaches saturation in about 50 passes (1.5 μsec for an rf frequency of 400 MHz or 3 μsec for an rf frequency of 200 MHz) for the FEL to reach the steady-state power level of 1 MW. In a combat environment, this is essentially an instantaneous engagement.

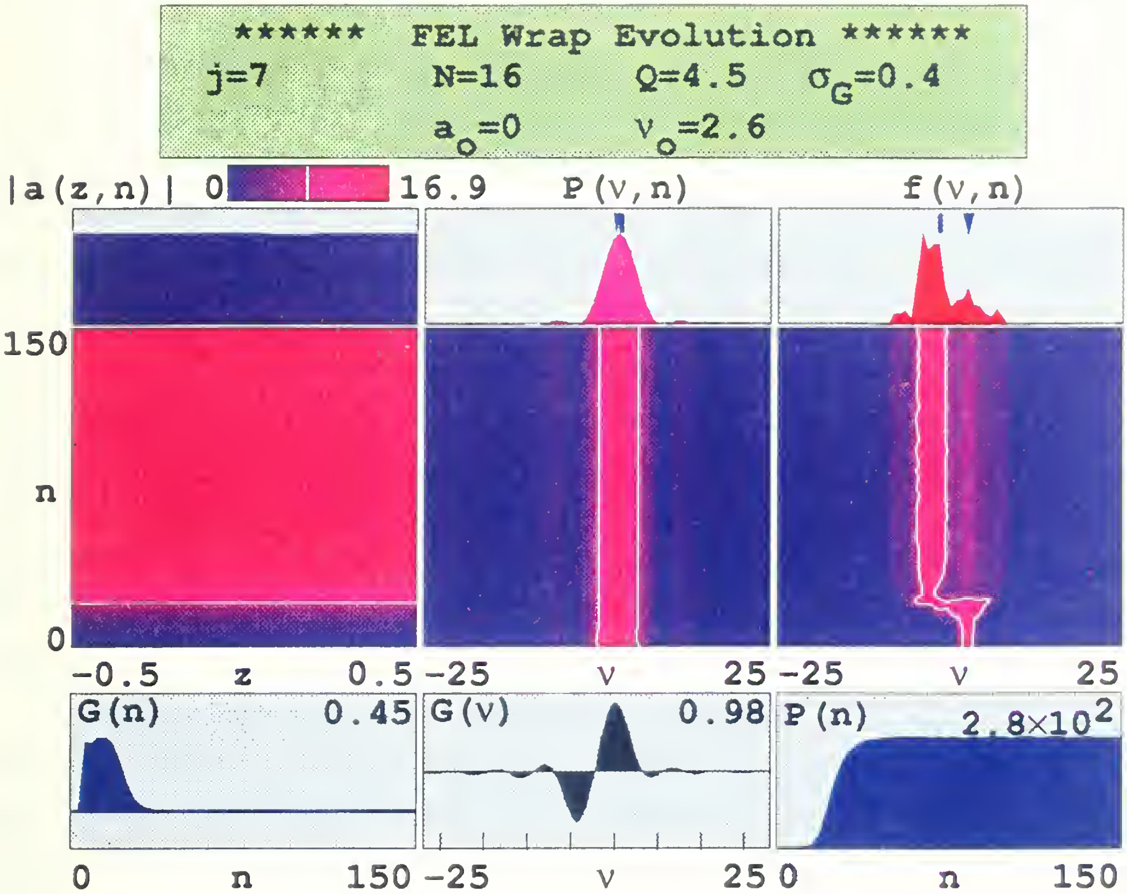

Figure 20 - Optical field characteristics at saturation for operation at λ = 3 μm

C. FEL OPERATION - 10 μm WAVELENGTH

In the maritime environment, there are two principal wavelength bands in the infrared (IR) suitable for laser propagation. These are the 3-5 μm short wave infrared (SWIR) and the 8-12 μm long wave infrared (LWIR) bands. Now that operation at 3 μm with a 1 MW output has been demonstrated, operation in the LWIR band at a wavelength about 10 μm, using the same undulator, is explored.

To maintain resonance at λ = 10 μm, the beam energy must be reduced to 54.8 MeV. The dimensionless current and optical mode waist are now j = 13 and w_o = .66 mm, respectively. If we lay a curve corresponding to a 1 MW output with the new parameters on top of Figure 17, we find that $|a| \approx 30$ and $Q \approx 4.5$. Therefore, if the resonator optics can be

made to have the same outcoupling at the LWIR wavelengths, the same undulator and resonator cavity could be used to operate in both bands.

The simulation results equivalent to Figures 18, 19, and 20 reveal only a few characteristics different than for the $\lambda = 3\mu m$ case. There are four principal longitudinal modes excited by the micropulses. Therefore, there is a modulation on the complex field envelope. This results in a startup time increase for the FEL of a factor of three. These features, while interesting, do not affect the engineering and feasibility results of concern in this analysis.

Despite the apparent wide bandwidth in operating wavelengths, there are many repercussions which must be considered. First, to reduce the beam energy by about one-half, the accelerator E is reduced in half. Therefore, the energy storage in each accelerator cavity is reduced by a factor of four. This means that $\Delta U/U$ increases by a factor of four resulting in an equal fractional increase in the rf field distortions caused by an accelerating micropulse. This will likely be unsatisfactory for proper beam transport in RT cavities. SC cavities will be more resistant to this effect.

A second consideration is the optical mode size with respect to the undulator gap distance. In the event of perfect alignment, the undulator will not penetrate into the Gaussian profile of the optical energy. However, if the alignment is off by as little as 1 mm, the undulator end magnets will penetrate into space normally occupied by several kilowatts of power. This can be compensated for by increasing the undulator gap distance. However, as a result of the corresponding changes in the undulator parameters, the undulator will be longer, have an increased sensitivity to electron beam quality, and the Q value of the optical resonator will increase. This will increase the power density incident on the mirrors for the same mirror separation. Therefore, if operation in the LWIR is desired, this tolerance must be considered when finalizing the undulator and resonator design.

D. RESONATOR OPTICS

One of the principal disadvantages of the FEL for use as a laser weapon is that the optical waist is very small. Therefore, the power density incident on the resonator optics is large. Figure 21 shows the average power density incident on the resonator mirrors as a function of mirror separation for the undulator with λ_o = 3 cm and N = 16. With an 18 meter mirror separation, the mirror power density is 70 kw/cm^2 at $\lambda = 3$ µm and 20 kW/cm^2 at $\lambda = 10$ µm. Modern optical components can support a power density in excess of 100 kW/cm^2 [51].

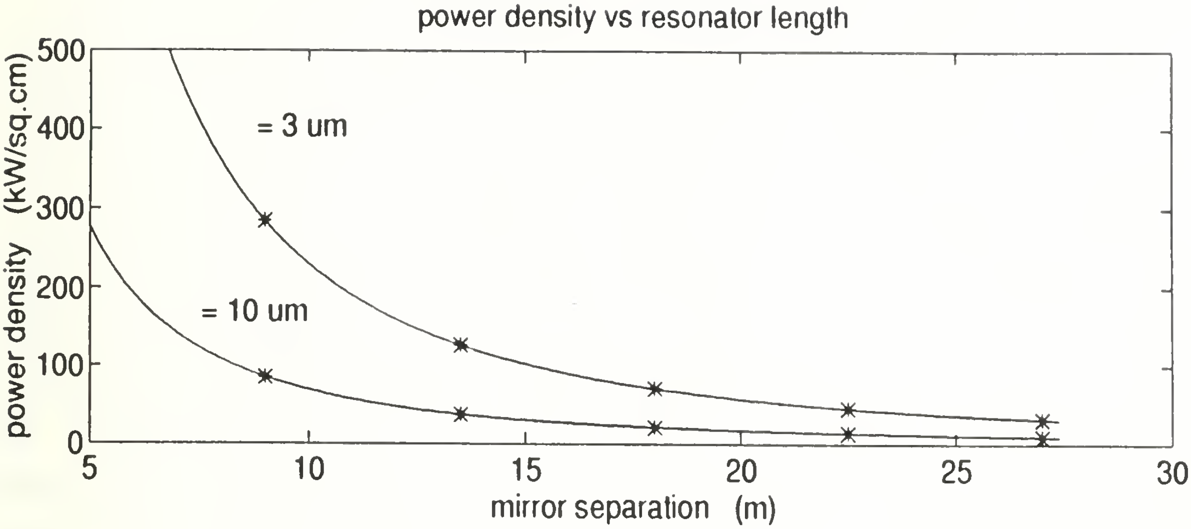

Figure 21 - Power density on the resonator mirrors for operation at $\lambda = 3\ \mu m$ and $\lambda = 10\ \mu m$ (* - denotes allowable mirror placements consistent with the rf frequency choices in Table 7)

In the shipboard environment, space and volume allocation is of particular concern to the ship design engineers. The mirror power density limitations require that the mirrors be about 18 m apart. However, it may be possible to reduce the resonator length with mirrors that exceed the 100 kW/cm^2 performance level. While this is a considerable length within the ship, the actual volume of the resonator is quite small since the optical mode can be contained within a cross-section of about 20 cm. The hardware for the active stabilization of the optics to maintain resonator alignment during ship vibrations, flexing, and torsional rotations will constitute the bulk of the resonator volume. Therefore, the only significant amount of space that will be needed will be at the mirror locations themselves.

VI. CONCLUSIONS AND RECOMMENDATIONS

The FEL is a promising candidate for a possible high-average power shipboard laser weapon. Unlike other candidates, such as chemical lasers, the FEL is electrically powered. An additional electrical power distribution bus would be required aboard a ship if an FEL weapon was to be deployed.

An FEL with a 1 MW laser output would require 6-10 MW of electrical power from the prime power distribution system. A gas turbine naval engineering plant could be modified to supply this power. Power from a propulsion turbine could be diverted to power the dedicated FEL distribution bus. The added distribution system would increase the ship's displacement by 22 tons and require 22 m^3 of the ship's volume to implement. The power supply that powers the rf sources for the linear accelerator were rated at an output voltage of 100 kV and an output power of 10 MW. This power supply is only 82% efficient and requires a large external cooling capability. The efficiency can be improved, however, with the development of alternative rf sources which operate at half of this voltage. The development of these alternate rf power supplies is recommended.

The linear accelerator driving the FEL would employ energy recovery to increase the power efficiency and reduce the operating radiation levels. Consequently, the electron beam has a large average current. Furthermore, the accelerator would operate at lower rf frequencies than most linear accelerators. Therefore, the electron pulse lengths are longer than those commonly used in most FELs. The high-average current and long pulse lengths reduce the number of undulator periods required to extract the 1 MW output power from the electron beam. Therefore, the FEL has a low sensitivity to electron beam quality.

The FEL examined in this thesis requires further development before it can be built. Some of the technologies that require further development are: energy recovery employment, control system requirements, and the accelerator electron injector output capacity. Additional experiments are needed to determine the limitations of energy recovery including rf phase and amplitude stability requirements as a function of FEL undulator energy extraction efficiency. Control systems are required to regulate the input power to rf sources and the rf input to accelerator components. Additional work is necessary to adequately control the electron beam transport instabilities that will result from high-average currents. Finally, electron injector technology can currently produce average currents of tens of milliamps. Advancements are needed for the shipboard FEL weapon. Further development of these FEL technologies is recommended.

APPENDIX - POWER SUPPLY CALCULATIONS

This appendix outlines the procedure used to estimate the weight and volume of the FEL power supplies in Chapter IV. Only commercially available, off-the-shelf components were considered in the analysis. No attempt was made to determine the savings that may be possible with a product development program. Therefore, the results are a conservative estimate. The components selected in the analysis are meant to be representative components. It should not be assumed that these components are recommended for procurement. The voltage and current ratings for all of the components used in the analysis were derated by the Navy derating factor of 0.7. The dc link and filter components were not considered.

A. 100 KV, 3 PHASE, PHASE-CONTROLLED RECTIFIER

The functional circuit diagram for a 3 phase, phase-controlled rectifier is shown in Figure 22.

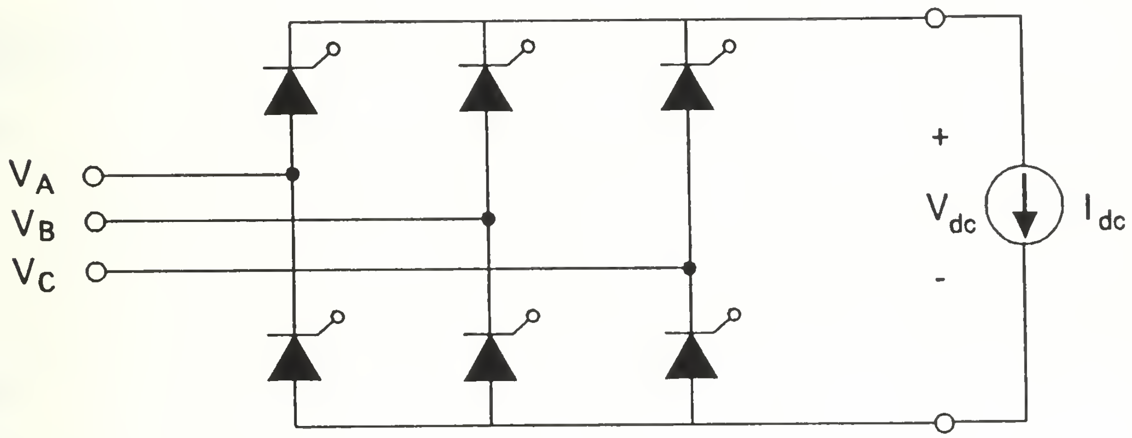

Figure 22 - Functional circuit diagram for a 3 phase, phase-controlled rectifier

Commercially available silicon controlled rectifiers (SCRs) are not rated to support a 100 kV blocking voltage. Several SCRs must be connected in series to accomplish the function of each SCR in Figure 22. Each of these series-connected SCRs must be protected with a snubber circuit and balancing resistor. The series connection of the SCRs is illustrated in Figure 23. Forced-commutation circuits for the SCRs are not included. It is assumed that the

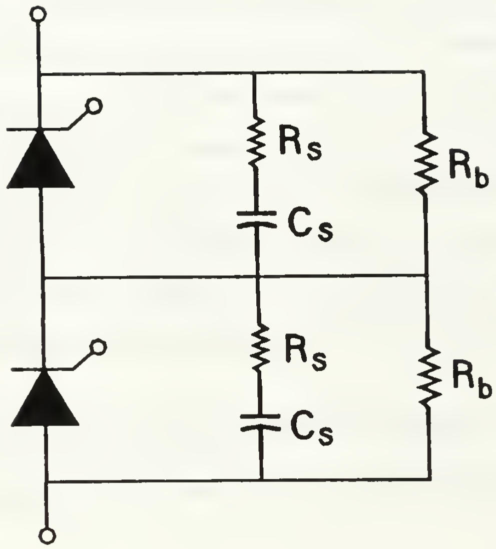

Figure 23 - Series-connected SCRs with protective balancing resistors and snubbers

blocking voltage is sufficient to rapidly reverse bias the SCRs.

1. SCR Selection

The rectifier has an output dc voltage, V_{dc}, of

$$V_{dc} = \frac{3}{\pi} V_m \cos \alpha = 100 \text{ k}V. \quad \text{(A.1)}$$

where V_m is the peak line-to-line input ac voltage and α is the SCR firing angle. Since the output dc voltage is reduced by only 13.4% when α is adjusted from 0-30°, V_m = 105 kV is chosen so that V_{dc} = 100 kV for α = 0°. To supply 10 MW of power, the output dc current, I_{dc}, must be 100 A. The peak reverse blocking voltage for the SCR, V_{rr}, is V_m and the conduction current, I, is 100 A. The derated values of V_{rr} and I are V_{drr} = 150 kV and I_d = 143 A, respectively.

Using Ref. [61], the SCR model T8K7 was chosen for the SCR component. The ratings of this SCR are listed in Table 14. The value V_{RRM} is the repetitive reverse blocking voltage, $I_{T(av)}$ is the peak average conduction current, I_{GT} is the gate current, I_{RRM} is the leakage current, I_{TSM} is the peak repetitive surge current, and t_d is the turn-on delay time of the SCR.

V_{RRM} (kV)	$I_{T(av)}$ (A)	I_{GT} (mA)	I_{RRM} (mA)
4.5	350	200	75

I_{TSM} (A)	t_d µsec	Weight (kg)	Volume (cm^3)
1500	2	0.227	72.9

Table 14 - Rating values for SCR model T8K7

Allowing for the failure of one SCR, 35 SCRs are required to construct each of the six branches in Figure 22. Therefore, a total of 210 SCRs are needed. The total SCR conduction losses are 19 kW.

2. Balancing Resistors

Balancing resistors are required to ensure that all series-connected SCRs block the same voltage. Otherwise, variations in leakage currents could cause an excessive voltage to build up across one SCR. The actual blocking voltage for each SCR is V_{block} = 3.1 kV. The value of R_b is calculated as

$$R_b = \frac{V_{block}}{10\, I_{RRM}} = 4\ \mathrm{k}\Omega \qquad \text{(A.2)}$$

The required power rating of this resistor is

$$P_{R_b} = \frac{V_d^2}{R_b} = 4.8\mathrm{kW} \qquad \text{(A.3)}$$

where V_d = 4.5 kV is the derated voltage rating of the SCRs. Multiple resistors will have to be placed in series to meet this power rating. From Ref [62], a suitable resistor is the type 270. The ratings of this resistor are listed in Table 15. The actual power dissipation of this

Power (kW)	Weight (kg)	Volume (cm^3)
1	0.28	1610

Table 15 - Rating values for the type 270 resistor

resistor is V_{block}^2/R_b = 2.4kW. One balancing resistor is needed for each series-connected SCR and five type 270 resistors are required per balancing resistor. Therefore, a total of 1050 resistors are needed with a total power dissipation of 500 kW.

3. Snubber Components

In this rectifier, the snubber provides voltage and current protection for series-connected SCRs during firing and turn-off. If one or more SCRs latch slower than the rest of the SCRs in a branch, an excessive voltage could be applied across these SCRs. The snubber capacitor provides the charge to the conducting SCRs during the period when these slower SCRs still have not latched. When the SCRs are first conducting, though, the capacitor would be effectively shorted causing a large current surge. The snubber resistor is placed in series with the capacitor to limit the discharge.

There is no definitive way to analytically determine rectifier snubber component values. However, a conservative methodology can be used to estimate these values with a design margin. The following method describes how the snubber component values were determined.

The latching delay time for the T8K7 SCR is 2 μsec. Assuming the snubber capacitor must supply the full conduction, the minimum capacitance necessary to store the required charge is

$$C_{s,min} = \frac{I_d \ t_d}{V_{block}} = 0.09 \ \mu F \ . \tag{A.4}$$

The snubber resistor must limit the capacitor current to within the surge current rating of the SCR. The derated surge current rating of the SCR, I_{dsm}, is 1050 A. The minimum snubber resistance is calculated by

$$R_{s,min} = \frac{V_d}{I_{dsm} - I_d} = 5\Omega \tag{A.5}$$

Assuming that the SCR switches instantaneously, the power rating of the snubber resistor is required to be

$$P_{R_s} = I_{rms}^2 R_s \approx \frac{V_d^2}{R_s}\left[\frac{R_s C_s f_{ac}}{2}\right] \tag{A.6}$$

where f_{ac} is the rectifier input ac frequency. Equations A.4, A.5, and A.6 include a margin of conservatism. The resistor power losses are independent of the resistance value but are directly proportional to the ac bus frequency. To minimize the power losses while maintaining the effectiveness of the snubber, the values of R_s = 5 Ω and C_s = 0.2 μF are required. The required voltage rating of the capacitor is 4.5 kV, and the resistor is to have a power rating of 3.2 kW. The value f_{ac} = 800 Hz is assumed.

From Ref. [63], a suitable capacitor design was selected. The capacitor ratings are listed in Table 16.

Voltage (kV)	Capacitance (μF)	Weight (kg)	Volume (cm^3)
4.5	0.2	0.43	400

Table 16 - Rating values for a 0.2 μF, 4.5 kV capacitor

There are 210 required snubber capacitors. Therefore, a total of 210 capacitors are required.

The type 270 was selected for the snubber resistor. Four type 270 resistors are needed for each snubber. Therefore, a total of 840 resistors are required. The power loss of each snubber resistor is $V_{block}^2 C_s f_{ac}$ = 1.54kW, so that the total power dissipation by all of the snubbers is 1290 kW.

4. SCR Gating Power Supply

A current pulse applied to the gate of an SCR is required in order for it to fire. The T8K7 SCR requires a current pulse of 200 mA and dissipates 5 W at the gate in order to fire. Since there are 35 SCRs in each of the six rectifier branches, a total of 7 A and 175 W is required to fire all of the SCRs in a branch. The derated values of required gate power supply current and power are 10 A and 250 W, respectively.

From Ref. [64], Acopian power supply model A28H1400 was selected. The ratings of this power supply are listed in Table 17.

Voltage (kV)	Current (A)	Power (W)	Weight (kg)	Volume (cm^3)
28	12	336	11.8	9900

Table 17 - Rating values for Acopian power supply model A28H1400

A total of six power supplies would be required.

B. VOLTAGE MULTIPLICATION CIRCUIT

The fundamental circuit diagram for a 500 kV voltage multiplier is shown in Figure 24. Figure 24 is an 8× voltage multiplier. An increased multiplication factor, F_v, is obtained by cascading additional stages. To obtain a 500 kV output with an input line voltage of 5 kV (rms), a multiplication factor of $F_v = 72$ is required. It is important to know that if any of these stages fail, the voltage multiplication factor is reduced by two. The next stage in the cascade must be rated to assume the load of the failed stage or it may also fail. Therefore, each diode and capacitor must be designed to the limiting position in the circuit. The diodes must be designed for a reverse blocking voltage of $2E_p$ and a current of $F_v I_{dc}$. The capacitors must be rated for a voltage of $3E_p$. The derated peak surge current, to which all of the circuit components must be rated, is given by

$$I_{dsm} = \frac{4\pi}{0.7} f_{ac} C E_p = 228.5A. \tag{A.9}$$

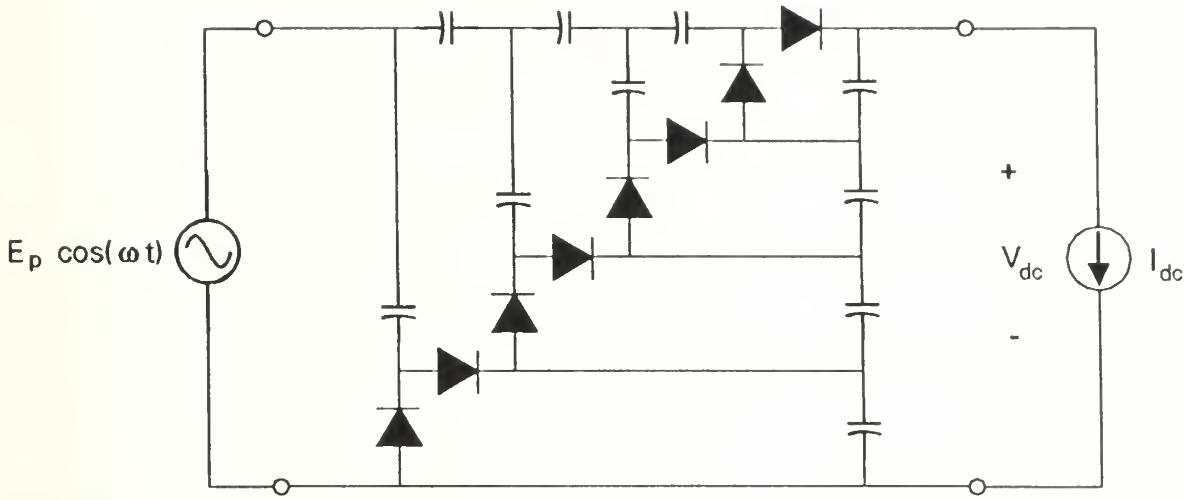

Figure 24 - Functional diagram for a voltage multiplier circuit

1. Capacitor selection

The effective output capacitance, C_{eff}, of the voltage multiplier needed to supply a current I_{dc} is given by

$$C_{eff} = \frac{I_{dc}}{f_{ac}\ \Delta V_o}, \tag{A.7}$$

where ΔV_o is the allowed output voltage ripple. The value C_{eff} of the circuit is

$$C_{eff} = 4\ C \frac{F_v - 1}{F_v (F_v - 2)}, \tag{A.8}$$

where C is the capacitance of each capacitor. Given values of f_{ac} = 800 Hz, I_{dc} = 500 mA, F_v = 72, and arbitrarily choosing ΔV_o = 5 kV, then each capacitor in Figure 24 must have a capacitance C = 2.25 μF. The derated voltage rating of the capacitors is 30.3 kV. The total number of these capacitors is $1.5F_v$ - 2 = 106 capacitors.

Using Ref. [63], capacitor model 30F1377 was selected for the capacitor component. The ratings of this capacitor are listed in Table 18.

voltage (kV)	Capacitance (μF)	Weight (kg)	Volume (cm^3)
30	2.37	19	11500

Table 18 - Rating values for capacitor model 30F1377

A total of 106 capacitors is required.

2. Diode selection

Each diode in Figure 24 must be rated for the limiting current and voltage values in the circuit. The required diode ratings are $I_d = F_v I_{dc}/0.7 = 51.4$ A, $V_{drr} = 20.2$ kV, and $I_{dsm} = 228.5$ A. Using Ref. [61], diode R4051070 was selected. The ratings of this diode are listed in Table 19.

V_{RRM} (kV)	$I_{T(av)}$ (A)	I_{TSM} (A)	I_{RRM} (mA)	Weight (kg)	Volume (cm^3)
1	70	1200	0.1	0.018	3.18

Table 19 - Rating values for diode R4051070

It is necessary to place several of these diodes in series to accomplish the function of each diode in Figure 24. Allowing for a single failure within the diode branch, 22 diodes are required per branch. There are F_v diode branches so that a total of 1584 R4051070 diodes are required. The total conduction losses are 50 kW.

3. Balancing resistor selection

The peak blocking voltage of each diode is $V_{block} = 2E_p/22 = 643$ V. Using equation A.2, the required value for the balancing resistor is $R_b = 643$ kΩ. The required power rating for this resistor is $V_d^2/R_b = 1.3$ W. Using Ref. [65], resistor 620KW-2-ND was selected. The ratings of this resistor are listed in Table 20.

Power (W)	Weight (kg)	Volume (cm^3)
2	0.01	0.4

Table 20 - Rating values for resistor 620KW-2-ND

One of these resistors is required for each of the R4051070 diodes. Each of these resistors dissipates $V_{block}^2/R_b = 0.64$ W. Therefore, 1584 resistors are required with a total power dissipation of 1 kW.

C. SUMMARY

The total weight, volume, and power losses for the 100 kV rectifier and 500 kV voltage multiplier power supplies are listed in Table 21.

	100 kV	500 kV	units
Weight	1500	4100	kg
Volume	8	3	m^3
power losses	1800	50	kW

Table 21 - Power supply summary

The weight estimate was made by multiplying the component totals by a factor of two. Power supplies that operate above about 40 kV are required to have enclosures which are filled with high voltage oil, SF_6, or some other means of protection between components. Due to the large amount of heat losses, the 10 MW power supply is assumed to be filled with oil which can also be used as a cooling medium. The 500 kV power supply will need high voltage shielding to isolate it from the environment. The volume estimates include a stacking factor of 2.5. This factor accounts for the high voltage shielding and unused space within the power supply after the components are assembled.

The power efficiency of the 10 MW power supply is about 82%. While this is acceptable for desktop size electronics, the 1.8 MW of power losses place an added design burden of forced cooling for the power supply. The efficiency of the power supply can be increased significantly with the development of alternative accelerator rf sources, as described in Chapter III, which operate at substantially lower voltages.

LIST OF REFERENCES

[1] J. M. J. Madey, "Stimulated Emission of Radiation in Periodically Deflected Electron Beams," *Journal of Applied Physics*, vol 42, 1971

[2] "High-Power Ultraviolet and Infrared Free-Electron Laser for Industrial Processing," The Laser Processing Consortium, Continuous Electron Beam Accelerator Facility, Newport News, VA, May 1994

[3] D. D. Quick, "Simulations of the High Average Power Selene Free Electron Laser Prototype," Master's Thesis, Naval Postgraduate School, Jun 1994

[4] W. F. Wilkenson, "A Theory for Optical Wavelength Control in Short Pulse Free Electron Laser Oscillators," Master's Thesis, Naval Postgraduate School, Jun 1993

[5] W. B. Colson, "Classical Free Electron Laser Theory," Chapter 5 in the *Free Electron Laser Handbook*, W. B. Colson, C. Pellegrini, and A. Renieri, editors, North-Holland Physics, Elsevier Science Publishing Co, The Netherlands, 1990

[6] A. Yariv, *Quantum Electronics*, third edition, John Wiley and Sons, NY, 1991

[7] J. D. Jackson, *Classical Electrodynamics*, second edition, John Wiley & Sons, NY, 1963

[8] W. B. Colson, "The Nonlinear Wave Equation for Higher Harmonics in Free-Electron Lasers," *IEEE Journal of Quantum Electronics*, vol QE-17, no 8, Aug 1981

[9] NBS Publication 380, Supplement 1, "Photonuclear Data Index 1973-1977," U.S. Department of Commerce National Bureau of Standards, issued Aug 1978

[10] J. A. Edighoffer et al, "A Computer Model of the Energy-Current Loss Instabilities in a Recirculating Accelerator System," *Proceedings of the* 16^{th} *Annual FEL Conference*, Stanford University, 22-26 Aug 1994

[11] W. B. Colson et al, Presented at the 16^{th} Annual FEL Conference, Stanford University, 22-26 Aug 1994

[12] Private communication with G. R. Neil, Continuous Electron Beam Accelerator Facility

[13] V. N. Litvinenko et al, "Component Technologies for a Recirculating Linac Free-Electron Laser," SPIE Laser Power Beaming, Technical Conference 2121, Los Angeles, CA. 27-28 Jan 94

[14] Private Communication with G. R. Neil, H. Liu, S. V. Benson, J. Benasch, and S. Simrock at the Continuous Electron Beam Accelerator Facility, 25-26 Jul 1994

[15] J. Kirchgessner, "The Use of Superconducting RF for High Current Applications," Laboratory of Nuclear Studies, Cornell University, Ithaca, NY

[16] H. Padamsee et al, "Physics and Accelerator Applications of RF Superconductivity," *Annual Review of Nuclear Particle Science*, vol 43 (1993)

[17] C. H. Rode et al, "Cryogenic Optimization for Cavity Systems," Continuous Electron Beam Accelerator Facility, Newport News, VA

[18] J. F. Schmerge et al, "An Accelerator/Wiggler for High Efficiency FEL Operation," *Nuclear Instruments and Methods in Physics A* 341 (1994)

[19] J. Kirchgessner et al, "Superconducting RF Activities at Cornell University," Laboratory of Nuclear Studies, Cornell University, Ithaca, NY

[20] K. J. Kim et al, "An Infrared Free Electron Laser System for the Proposed Chemical Dynamics Research Laboratories at LBL based on a 500MHz Superconducting Linac," *Nuclear Instruments and Methods in Physics A* 341 (1994)

[21] J. I. M. Botman et al, "Developments of the TEUFEL Injector Racetrack Microtron," *Nuclear Instruments and Methods in Physics A* 341 (1994)

[22] P. M. Lapostolle, *Linear Accelerators*, John Wiley & Sons, NY, 1970

[23] J. M. Watson, "Specification for FEL Space System Linac," Los Alamos National Laboratory, Los Alamos, N.M., 6 Dec 1982

[24] A. M. Vetter, Private Communication, letter dated 3 Jun 94

[25] M. Takao et al, "Recirculation Scheme in the Second Phase of the JAERI FEL project," *Nuclear Instruments and Methods in Physics A* 341 (1994)

[26] D. C. Nguyen et al, "Initial Performance of the Los Alamos Advanced Free Electron Laser," *Nuclear Instruments and Methods in Physics A* 341 (1994)

[27] *CRC Handbook of Chemistry and Physics*, 62^{nd} edition, CRC Press Inc, Boca Raton, FL, 1982

[28] R. Zhang et al, "A Millimeter Wave FEL Driven by a Photocathode RF Linac," *Nuclear Instruments and Methods in Physics A* 341 (1994)

[29] M. Qian et al, "Photoemission Studies on LaB_6 and Metals using Nanosecond KrF Excimer Laser," *Proceedings of the* 16^{th} *Annual FEL Conference*, Stanford University, 22-26 Aug 1994

[30] A. Agafonov et al, "Linac Driver for the FEL Project at P. N. Lebedev Institute," *Nuclear Instruments and Methods in Physics A* 341 (1994)

[31] I. S. Lehrman et al, "Design and Construction of a Compact Infrared FEL," *Nuclear Instruments and Methods in Physics A* 341 (1994)

[32] M. Fujita et al, "Photoinjector for a 6MeV S-band RF Linac at ILT/ILE Osaka University," *Nuclear Instruments and Methods in Physics A* 341 (1994)

[33] S. H. Kong et al, "Performance of Cesium Telluride Photocathodes as an Electron Source for the Los Alamos FEL," *Proceedings of the* 16^{th} *Annual FEL Conference*, Stanford University, 22-26 Aug 1994

[34] S. H. Kong et al, "Fabrication and Characterization of Cesium Telluride Photocathodes: A Promising Electron Source for the Los Alamos FEL," *Proceedings of the* 16^{th} *Annual FEL Conference*, Stanford University, 22-26 Aug 1994

[35] S. H. Kong et al, "Photocathodes for Free Electron Lasers," *Proceedings of the* 16^{th} *Annual FEL Conference*, Stanford University, 22-26 Aug 1994

[36] R. F. X. A. M. Mols et al, "Performance of a MOPA Laser System for Photocathode Research," *Nuclear Instruments and Methods in Physics A* 341 (1994)

[37] B. E. A. Saleh et al, *Fundamentals of Photonics*, John Wiley & Sons, NY, 1991

[38] R. Beach et al, "Scalable Diode-End-Pumping Technology Applied to a 100 mJ Q-Switched Nd:YLF Laser Oscillator," *Optics Letters*, vol 18 no 16, Aug 1993

[39] A. Yariv, *Optical Electronics*, fourth edition, Holt, Rinehart, and Winston, NY, 1991

[40] P. R. Claisse et al, "Internal Quantum Efficiency of Laser Diodes," *Electronics Letters*, vol 28, no 21, Oct 1992

[41] H. Plaessmann et al, "Multipass Diode-Pumped Solid State Optical Amplifier," *Optics Letters*, vol 18, no 17, Sept 1993

[42] R. F. X. A. M. Mols et al, "Parametric Study of the behavior of Group Velocity Dispersion in Optical Pulse Compression," *Optics Communications*, 94 (1992)

[43] T. Graf et al, "High Power Nd:YLF Laser End Pumped by a Diode-Laser Bar," *Optics Letters*, vol 18, no 16, Aug 1993

[44] CERN Accelerator School, *RF Engineering for Particle Accelerators*, Exeter College, Oxford, UK, 3-10 Apr 91

[45] A1A-K3513 Issue 1, Data Sheet for Continuous Wave Power Amplifier Klystron K3513, EEV Ltd., Essex, England, Aug 1993

[46] C. Bearzatto et al, "Advantages of Multiple Beam Klystrons (MBK)," Thompson Tubes Electroniques, Velizy, France, May 1992

[47] R. D. Peters et al, "The Klystrode IOT - A New, Compact, High-Efficiency Electron Tube," Varian Associates, San Carlos, CA

[48] private communication with S. Lenci, Varian Associates, San Carlos, CA

[49] private communication with S. L. Hesselsohn, EEV Inc., Elmsford, NY

[50] J. M. Herbelin et al, "Development of Laser Mirror of Very High Reflectivity using the Cavity-Attenuated Phase-Shift Method," *Applied Optics*, vol 20, 1 Oct 81

[51] private communication with S. Siahatgar and J. Albertine, Space and Naval Warfare Systems Command, Arlington, VA

[52] T. J. Doyle et al, "Propulsion Powered Electric Guns - A Comparison of Power System Architectures," DTRC-PAS-91-31, David Taylor Research Center, Jul 1991

[53] S. Fish et al, "Initial Impact Assessment of Electro-Thermal-Chemical Gun Outfit Aboard the DDG-51 with Mechanical Drive," DTRC-PAS-91-53, David Taylor Research Center, Feb 1992

[54] P. A. Dent et al, "Advanced Strike Platform (ASP) Concept: Feasibility Assessment of a Linear Induction Electromagnetic Launcher on a Naval Surface Combatant," DTRC/SD-91-05, David Taylor Research Center, Jun 1991

[55] A. M. Trotta et al, "Pulse Power System Component Study," DTRC-TM-27-90-40, David Taylor Research Center, 14 Dec 1990

[56] G. F. Grater et al, "Design Considerations Integrating ETC Gun Systems Aboard Naval Surface Combatants," *Naval Engineers Journal*, vol 106, no 3, May 1994

[57] A. S. Gilmour, "Power Conditioning Systems for High-Power, Airborne, Pulsed Applications," *IEEE Transactions on Aerospace and Electronic Systems*, vol AES-13, no 6, Nov 1977

[58] private communication with Guy F. Grater, Pulsed Power Systems Office, Naval Surface Warfare Center, Annapolis, MD

[59] K. Halbach, "Permanent Magnet Undulators," *Proceedings of the Bendor Free Electron Laser Conference*, Les Editions de Physique, Bendor, France, 26 Sep - 1 Oct 1982

[60] private communication with Dave Quimby, Spectra Technology Inc., Seattle, WA. 31 Oct 94

[61] *Rectifier and Thyristor Applications and Technical Data Book*, first edition, Powerex, Inc. Aug 1993

[62] "Type 200, Type 270 Data Sheet," facsimile from Ohmite Manufacturing Company, 7 Dec 1994

[63] private communication with D. Seymour and R. Patton, General Electric Capacitor, facsimile with design specifications for high energy storage capacitors, 12 Dec 1994

[64] *Acopian Power Supply Catalog, 1994*, Acopian, 1994

[65] *Digi-Key Catalog No. 943*, Digi-Key Corporation, May-Jun 1994

INITIAL DISTRIBUTION LIST

1.	Defense Technical Information Center Cameron Station Alexandria, Virginia 22304-6145	2
2.	Dudley Knox Library, Code 52 Naval Postgraduate School Monterey, California 93943-5101	2
3.	Professor William B. Colson, Code PH/Cw Chairman, Department of Physics Naval Postgraduate School Monterey, California 93943-5117	6
4.	Chairman, Code EC Department of Electrical and Computer Engineering Naval Postgraduate School Monterey, California 93943-5121	1
5.	Professor Michael Morgan, Code EC/Mw Department of Electrical and Computer Engineering Naval Postgraduate School Monterey, California 93943-5121	1
6.	Professor Robert Armstead, Code PH/Ar Department of Physics Naval Postgraduate School Monterey, California 93943-5117	1
7.	Professor Robert Ashton, Code EC/Ah Department of Electrical and Computer Engineering Naval Postgraduate School Monterey, California 93943-5121	1
8.	Professor Karlheinz Woehler, Code PH/Wh Department of Physics Naval Postgraduate School Monterey, California 93943-5117	1

9. Professor Ron Pieper, Code EC/Pr 1
Department of Electrical and Computer Engineering
Naval Postgraduate School
Monterey, California 93943-5121

10. John Albertine 1
Code 332, Division Director
Directed Energy Division
Space and Naval Warfare Systems Command
2451 Crystal Dr.
Arlington, Virginia 22245-5200

11. Dr. George Neil 1
CEBAF
12000 Jefferson Ave.
Newport News, Virginia 23606

12. Lieutenant Robert Lyon, USN 2
1050 Kensington Dr.
Roseville, California 95661